JOURNAL OF GEOPHYSICAL RESEARCH, VOL. 105, NO. A8, PAGES 18,609–18,637, AUGUST 1, 2000

Upper atmospheric observations at the Arecibo Observatory: Examples obtained using new capabilities

B. Isham,[1] C. A. Tepley, M. P. Sulzer, and Q. H. Zhou
Atmospheric Sciences Group, Arecibo Observatory, Arecibo, Puerto Rico

M. C. Kelley[2]
Department of Electrical Engineering, Cornell University, Ithaca, New York.

J. S. Friedman and S. A. González
Atmospheric Sciences Group, Arecibo Observatory, Arecibo, Puerto Rico

Abstract. The Arecibo Observatory will soon complete a major instrumental upgrade which will provide improved capabilities for observations of the upper atmosphere. As in the past, Arecibo capabilities center on 430-MHz incoherent scatter radar (ISR) measurements of the ionosphere made locally or in conjunction with other national and international incoherent scatter facilities; the upgrade will add the capability for simultaneous two beam incoherent scatter observations and will extend plasma line measurements to ±15 MHz. Aeronomical studies may also be performed using a 46.8-MHz coherent scatter radar, the feed of which is coaxial with the 430-MHz line feed, the newly refurbished medium-frequency (MF) radar facility, and a new digital ionosonde. The original airglow laboratory continues to house the Fabry-Perot interferometers, Ebert-Fastie spectrometer, and tilting filter photometers used for observations of mesospheric, thermospheric, and exospheric airglow, while a new laboratory provides a permanent home for the lidars used for resonance fluorescence observations of atomic metal layers in the mesopause region and for Doppler Rayleigh measurements of the upper stratosphere and lower mesosphere. Finally, the recently upgraded high-frequency, high-power transmitter facility has performed active aeronomical and plasma physical studies alone and in conjunction with other Arecibo and visitor-supplied instruments. Observations performed as the upgrade nears completion have already provided a first look at what lies ahead in areas as diverse and fundamental as the structure and dynamics of the turbopause, the properties of upper atmospheric tides, the electrodynamics of the E and F regions, the dynamics of light ions in the topside, and the physics of plasma turbulence. Examples of these and other observations are presented, and the opportunities for future investigations are discussed.

1. Introduction

Incoherent scatter radar (ISR) observations have been carried out at Arecibo since the initial construction of the observatory was completed in 1963 [*Gordon*, 1964]. The principle radar frequency was then and is still 430 MHz, although during the 1960s ISR and other radar measurements were also performed at 40 MHz [*Watkins*, 1967; *Parrish*, 1968]. Optical observations at Arecibo began in 1967 using a 6300-Å photometer and, in 1968, a Fabry-Perot interferometer [*Wickwar*, 1971].

A first major upgrade in the early 1970s was primarily aimed at improving the surface of the 305-m dish in order to extend the frequency range for radio astronomy use [*LaLonde*, 1974]. At that time a 2380-MHz radar was added to allow for improved planetary radar observations [*Ostro*, 1993]; this radar has also been used for stratospheric observations [*Woodman*, 1980; *Ierkic et al.*, 1990]. In addition, the first high-frequency (HF) radio wave ionospheric interaction experiments at Arecibo were carried out in 1971 using an HF feed mounted above the dish [*Gordon et al.*, 1971]. These experiments led to the construction in the late 1970s of a

[1] Now at Department of Natural Sciences and Mathematics, Interamerican University, Bayamón, Puerto Rico.

[2] Also at Atmospheric Sciences Group, Arecibo Observatory, Arecibo, Puerto Rico

Paper number 1999JA900315.
0148-0227/00/1999JA900315$09.00

dedicated high-power HF transmitting facility, located 17 km NNE of the radar [*Fejer et al.*, 1985].

In 1985 a 46.8-MHz coherent scatter radar was added to the instrument cluster at the focus of the dish [*Röttger et al.*, 1986], and in 1986 the feed was redesigned to allow colinear 46.8- and 430-MHz observations (R. W. Sisk, private communication, 1997). This radar is used for mesosphere-stratosphere-troposphere (MST), HF interaction, meteor, and thunderstorm observations. In 1989, Arecibo acquired a 1.95-MHz medium-frequency (MF) radar for performing partial reflection spaced antenna drift observations of winds, tides, and planetary waves between 60 and 100 km altitude [*Reid*, 1988]. The MF radar is located 40 km WNW of the observatory and is maintained and operated in collaboration with the University of Puerto Rico at Mayagüez. In 1995 a cooperative project between scientists from Arecibo and the universities of Nebraska, Clemson, and Cornell resulted in the installation of a 430-MHz three-element Yagi interferometric receiving array near the main dish for use in observing the three-dimensional structure of winds and turbulence between 3 and 10 km altitude [*Palmer et al.*, 1997].

Since 1994 the Arecibo Observatory has been in the midst of a second major upgrade aimed at improving the feed system for the main 305-m antenna [*Kildal et al.*, 1991, 1994]. In addition, a ground screen has been added to reduce receiver noise caused by spillover, and a new 2380-MHz transmitter has been installed with over twice the power (1 MW CW) of the previous system [*Goldsmith*, 1996]. The ground screen has reduced the system temperature of the 430-MHz receiver by 20 K, to ~75 K. Beginning in 2000, the new Gregorian feed will allow two-beam 430-MHz ISR ionospheric measurements, will improve the F region plasma line measurement bandwidth from ±7.5 to ±15 MHz, and will allow focusing of the radar beam in the near field, which for the Arecibo 430-MHz radar is below 144 km [*Kildal and Davis*, 1996]. A parallel upgrade of the transmission lines at the Arecibo HF facility was also performed which resulted in a doubling of the transmitted HF power, and the MF radar data taking and control system has been enhanced, allowing a greater dynamic range in the sampled data and for remote operation via the Internet. In addition, construction of a second optical building to house two new resonance fluorescence lidar systems and the Doppler Rayleigh lidar has recently been completed. The resonance lidars are used primarily to study the dynamics and chemistry of the mesosphere by making high spatial and temporal resolution density measurements of the atomic metals found in a layer extending between roughly 80 and 105 km [*Beatty et al.*, 1989; *Castleberg*, 1997]; a soon-to-be-online Doppler capability will permit wind and temperature measurements in the same region. The Doppler Rayleigh system is capable of measurements of neutral wind, absolute temperature, and relative density from the middle stratosphere through the lower mesosphere (~25 to 60 km in altitude) [*Tepley*, 1994; *Castleberg*, 1997; *Friedman et al.*, 1997]. These systems have also been used for a multiwavelength study of aerosols in the upper troposphere and lower stratosphere [*Castleberg*, 1997]. Equipment for passive airglow observations, including interferometers, spectrometers, and photometers, will continue to be housed in the original optical facility.

As the current upgrade nears completion, Arecibo is hoping to attract old and new users to take full advantage of the new observational capabilities. We are now well along the way toward the next solar maximum, and the observatory is ready to provide the user community with the tools needed for high-resolution observations of ionospheric structure, dynamics, and electrodynamics, including topics as diverse as turbulence, waves, and tides; variations in structure and composition driven by the seasons and the solar cycle; and the microscopic physics of the ionospheric plasma. Specific examples include, among others, studies of vertical ion velocities, planetary waves, ion rain, collisional damping of Langmuir waves, meteor physics, traveling ionospheric disturbances, and the dynamics of the sodium layer. These examples are intended to provide a thought-provoking glimpse of the potential of the upgraded facilities as well as a stimulus for the development of improved and entirely new investigations.

This report focuses on Arecibo capabilities and observations in the upper atmosphere, primarily between 60 and 2000 km. Descriptions and examples of the use of the facilities have been divided into sections covering the radars (the 430-MHz incoherent scatter radar, the 46.8-MHz coherent scatter radar, the 1.95-MHz partial reflection radar, and the digital ionosonde), airglow and lidar observations, and aeronomical and plasma physical studies using the high-frequency, high-power transmitting facility.

2. Radar Instrumentation and Observations

2.1. The 430-MHz Incoherent Scatter Radar

The Arecibo incoherent scatter radar combines the world's largest dish antenna, 305 m in diameter, with a powerful transmitter having 2.5 MW peak power and 6% duty cycle. In combination with the reduced receiver noise temperature of ~75 K made possible by the new ground screen, this results in an overall system sensitivity more than 100 times greater than that of most other ISR facilities. At full power the bandwidth of the transmitter allows a 1-μs minimum pulse, which translates into a potential 150-m range resolution. The minimum pulse repetition period is 700 μs; the maximum pulse length is 2000 μs. The transmitter is housed on the ground next to the control room, and power is delivered to the feed system via a 450-m-long waveguide.

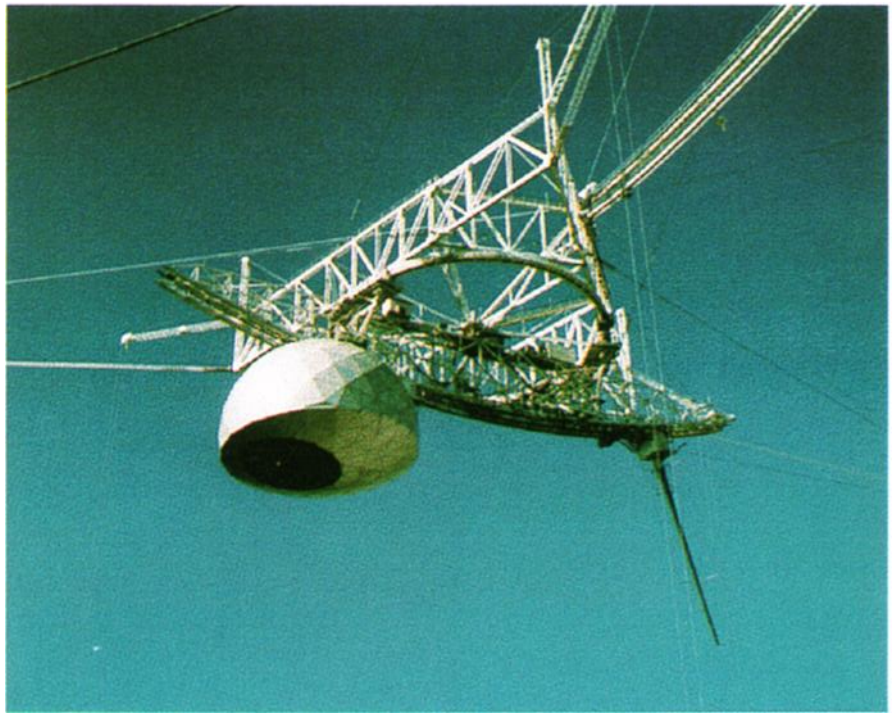

Plate 1. A recent view of the Arecibo feed platform showing the original 430 MHz line feed and the new Gregorian feed, which operates between 300 MHz and 10 GHz; beginning in 2000, both will be used for 430-MHz transmissions. The line feed is narrowband and typically cannot be used for plasma line observations near the F region peak; the Gregorian does not have this limitation. The two feeds each move on their respective sides of the azimuth arm, which limits the maximum zenith angle to ±20°. The azimuth arm can rotate up to 720° along a circular track attached to the triangular platform. The 900-ton platform is suspended 133 m above the 305-m dish by cables which pass over three towers and are anchored in concrete attached to the limestone bedrock.

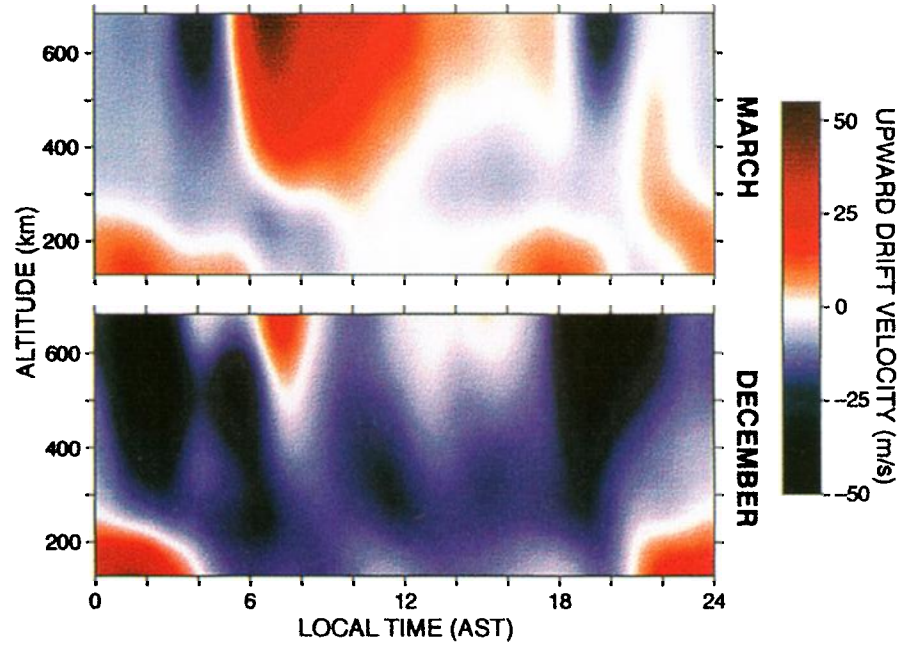

Plate 2. Average vertical ion drift over Arecibo versus time of day, altitude, and season. The average is over ~20 days of observations during each period, spread over a period of ~10 years ending in 1994. During the winter daytime the drift is due primarily to the meridional (northward) neutral wind, which forces the ions down the geomagnetic field and which is largely height-independent in the F region. During the night the ion drift is due to the meridional wind and also to ambipolar diffusion, which is a function of height, and thus so is the ion drift.

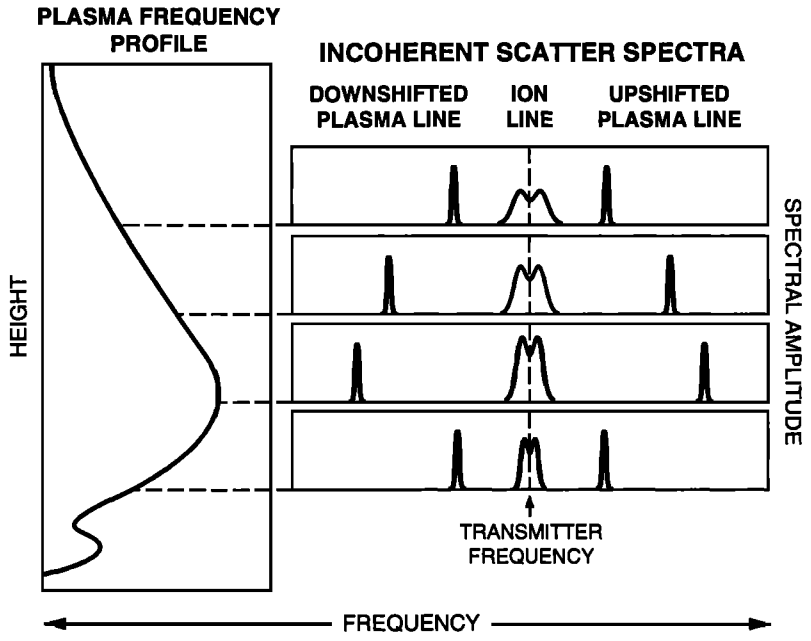

Figure 1. A schematic representation of the major features of the incoherent scatter radar spectrum and its relationship to the ionospheric plasma frequency profile. The ion and plasma lines arise from Bragg backscatter off thermal density fluctuations, the power of which is concentrated in the ion acoustic and electron Langmuir plasma wave modes, respectively.

In 2000, 430 MHz transmissions through the new Gregorian feed system, shown in Plate 1, will be possible. This will increase the bandwidth for incoherent scatter plasma line observations from 15 to 30 MHz and, with the concurrent use of the original 430-MHz line feed via splitting of the transmitted power, add a significant new capability for dual beam ISR observations. The Gregorian feed system will also allow near-field focusing of the 430-MHz radar beam via adjustment of the height of the Gregorian tertiary subreflector and of the reflector platform itself [*Kildal and Davis*, 1996]. Although the Gregorian has the advantage of larger bandwidth and focusing, the line feed makes more efficient use of the main dish when pointed vertically, as its radiation pattern fills the available aperture, while the Gregorian has an imprint diameter ~70% that of the 305-m reflector. Owing to the special design of the large Arecibo antenna and feed system, the pointing for both the line feed and the new Gregorian feed is restricted to a maximum of 20° from vertical [*Gordon*, 1964; *Davis*, 1997].

As shown in Figure 1, the principal features of the incoherent scatter spectrum are the ion line and the upshifted and downshifted plasma lines. These lines are due to Bragg scatter from thermal fluctuations in the ionospheric electron density. The ion line is due to scatter from fluctuations associated with ion acoustic waves and is routinely used to directly measure electron density, electron and ion temperatures, ion composition, and ion drift velocity [*Evans*, 1969]. The plasma line is due to scatter from fluctuations associated with electron plasma or Langmuir waves. During the day the plasma line spectrum is intensified by inverse Landau damping from photoelectrons and can be used to measure the electron density and the electron energy spectrum, and in the future we hope to be able to measure the thermal electron temperature and bulk electron drift velocity [*Yngvesson and Perkins*, 1968]. The nighttime plasma line is present at or slightly above the purely thermal level, which is ~1% that of the ion line intensity [*Carlson et al.*, 1982]; the weakness of the line along with the rapid change in plasma line frequency with altitude makes detection difficult. Although ionospheric incoherent scatter is associated with thermally excited plasma wave modes, the fundamental mechanism is that of Thomson scatter from individual electrons [*Thomson*, 1906; *Gordon*, 1958]. It should be noted that other types of scattering may also be detected with this radar, for example, those associated with stratospheric clear air turblence [*Sato and Woodman*, 1982] and meteors, the latter of which is discussed in detail in section 2.9.

Since 1994 the incoherent scatter radar control and data taking system has also been upgraded. The transmitter waveform is now programmable in amplitude, frequency, and phase, and the transmitter pulse may be sampled and recorded. As in the past, 12-bit A/D conversion is the standard and is normally used, but 8-, 4-, 2-, and 1-bit conversion may also be chosen. In addition, the maximum complex sampling frequency has been increased from 1 to 10 MHz. The maximum average recorded data rate per tape drive is slightly greater than before at ~400 kbytes/s, and the overall recorded data rate may now be increased to several times the sin-

gle tape value via data striping to several tape drives simultaneously. Finally, the radar data-taking modes, discussed in section 2.2, may be interleaved in multiples of either the integration period (timescales of seconds) or the pulse repetition period (timescales of milliseconds); this is taken advantage of in many experiments, a particular example being the world day observations discussed in section 2.6.

2.2. Incoherent Scatter Data Taking Modes

There are six incoherent scatter data-taking modes currently in use at Arecibo. All modes are optimized to take full advantage of Arecibo ISR sensitivity. Because of this, many of the capabilities of each of these modes are unique to the Arecibo radar. The parameters given for each mode are either standard or typical values, all of which can be adjusted at any time before or during an experiment.

2.2.1. Topside. The topside mode uses the ion line to measure properties of the ionospheric plasma up to 4000 km in altitude. In the standard configuration, a 500-μs pulse is transmitted every 20 ms, and parameters are measured between 255 and 2600 km. Although range gates are computed every 38 km, the true range resolution, 75 km, is determined by the 500-μs pulse length. Because of this, at altitudes near 255 km, accurate parameters often cannot be measured as the pulse is too long to resolve the short scale heights found at those altitudes and below. However, the lower heights are included in the program for those instances when conditions are favorable; equally or more important, they provide a measure of the electron density at the F region peak which can then be used to calibrate the data by comparison with simultaneous ionosonde measurements. At higher altitudes where scale heights are long, range resolution can be sacrificed to improve the signal-to-noise ratio, and the data can be averaged over height to improve the accuracy of the calculated parameters.

The data are sampled at 4 μs in quadrature, providing a 250-kHz bandwidth which is divided into two halves of 125 kHz each. This is because the transmitter center frequency alternates between plus and minus 62.5 kHz from band center during alternate pulse repetition periods, in effect making two receiver channels each having twice the nominal 20-ms pulse repetition period. The signal data come from the channel in which the transmitter is pulsed, while the noise data come from samples taken near 40 ms (6000 km) gate delay in the unpulsed channel. In this way the need to take long-gate-delay noise samples in the data channel is avoided, and the transmitter duty cycle can be kept at the reasonably high level of 2.5%. The 125-kHz bandwidth is enough to span even the widest spectrum due to H^+.

In order to limit the errors in the parameter calculations to reasonable values the topside data are typically averaged for 10 min and often 30 min at the higher heights where the signal-to-noise ratio is poor. On occasion, when the electron and ion temperatures are especially low, the spectra will be narrow, resulting in more power in each frequency bin, which increases the signal-to-noise ratio and allows shorter integration times. Typical electron, O^+, and H^+ temperature errors in the lower topside are around 30 K; the longer time and altitude averages commonly used at the higher altitudes can give error bars of about 100 K at 2000 km. Electron density and O^+, He^+, and H^+ composition errors of a few percent are common. Topside data are normally taken with the radar pointing vertically, and the vertical velocities of O^+ and H^+ can be measured separately at altitudes up to 1000 km wherever sufficient concentrations of the respective ions are present. The typical error in the lower topside is 10 m/s. Temperature and velocity for He^+ are not computed due to generally low He^+ concentrations and the difficulty of separating its spectral component from those due to H^+ and O^+.

2.2.2. Multiple radar autocorrelation function. The multiple radar autocorrelation function (MRACF) mode derives its name from the multiple frequencies (currently 7) which, in the standard operating configuration, are transmitted simultaneously within a 250 kHz bandwidth. This is done in order to fully exploit the large signal-to-noise ratio, significantly >1, available in Arecibo middle F region observations. This is in contrast to the data taken in the topside mode, which normally has a low signal-to-noise ratio, significantly <1. It can be shown that once the signal-to-noise ratio surpasses 1, further increases provide very little improvement in parameters derived from model fits to the observed spectra. By dividing the transmitter power among several radar channels, however, the excess signal can in effect be used to obtain additional statistically independent data samples, which can be averaged to improve the signal-to-noise ratio by a factor equal to the square root of the relative increase in the number of independent samples. This is opposite to the low signal-to-noise case (<1), where a benefit is obtained when independent samples can be traded for an increase in the signal-to-noise ratio [*Sulzer*, 1986*a*].

The altitude range in which the MRACF mode is normally used extends from 140 to 680 km. As altitude increases, the signal-to-noise becomes comparable to 1 and the advantage of multiple frequencies is lost. At low altitudes the short scale heights make single pulse measurements impractical.

The MRACF mode makes measurements similar to the topside mode, gathering ion line data for use in computing ionospheric plasma parameters. A 308-μs pulse is transmitted every 10 ms, and the backscatter is sampled in quadrature every 4 μs, producing a 250-kHz bandwidth, which matches that used by the multiple frequencies sent out by the transmitter. Because the bandwidth is shared by several data channels, the bandwidth of each channel is normally too narrow to measure

the broad spectrum of H^+; this is another fundamental difference in the topside and MRACF modes. The H^+ density can, however, be computed from MRACF data by accounting for the increase in base level and aliasing of the spectra which occur when H^+ is present. As in the topside mode, range gates are calculated every 38 km, but the fundamental range resolution as determined by the transmitted pulse length is 46 km. Noise samples are taken at the end of the 10-ms pulse repetition period. The transmitter duty cycle is just under 3.1%.

MRACF data are typically averaged for 20 s, which yields errors in the computed O^+ temperature of 20 to 30 K. However, usable results can often be achieved with integration times of only a few seconds; this can be useful at times when the ionosphere is rapidly changing, such as sunrise or sunset. Electron densities and ion compositions can normally be obtained with accuracies of 1 or 2%. Oxygen ion vector velocities are obtained via azimuth scans. With the line feed alone, a full, 16-min, 360° azimuth scan is required to compute the three velocity components. With the two-beam capability that will be available when the Gregorian feed comes on line, this time will be reduced by half. The line-of-sight velocity error is 10 m/s at lower heights, assuming 20-s averaging.

2.2.3. Coded long pulse. Coded long pulse is a technique developed at Arecibo to obtain high-resolution ion and plasma line spectra [*Sulzer*, 1986*b*]. The code is used to randomize unwanted spectra from neighboring gates, thus allowing range resolution limited only by the bandwidth of the radar. The setup is easily configurable based on experimental requirements, and baud lengths as short as 1 μs, corresponding to 150 m range resolution, are often used.

For ion line measurements a pulse of length 400 μs with 8-μs bauds is typically transmitted every 10 ms, yielding a 4.0% duty cycle. The frequency resolution of the directly digitized data is then 2.5 kHz, height resolution is 1.2 km, and the time resolution for usable processed data can be as low as 10 s. Ion line spectra can be measured beginning at 90 km or below, where they may be used to estimate the ion-neutral collision frequency [*Dougherty and Farley*, 1963; *Hagfors and Brockelman*, 1971; *Zhou et al.*, 1997*c*]. Electron temperatures and oxygen ion temperatures and velocities are routinely obtained with this technique up to >200 km. In between these limits a 1-min integration can yield results accurate to 20 K for the temperatures, 5Above 200 km, signal-to-noise begins to drop, the scale height increases, and MRACF becomes the favored mode for ion line observations.

For plasma line observations a pulse length of 1 ms with 1-μs bauds is typically transmitted every 25 ms, yielding a 4.0% duty cycle. The frequency resolution of the directly digitized data is then 1 kHz, height resolution is 150 m, and time resolution is 2 s. Useful plasma line data may be taken throughout the bulk of the E and F regions, limited by low plasma densities at ~150 km and below and by $1/r^2$ losses at ranges beyond 400 km.

2.2.4. Pulse-to-pulse technique. In the pulse-to-pulse technique, one short pulse is transmitted each pulse repetition period (PRP). That pulse is then used to obtain one sample from each desired range during each PRP; the pulse repetition period thus becomes the effective sampling rate. For example, given a 4-μs pulse and a 1-ms PRP, a 100-pulse-long fast Fourier transform (FFT) will produce spectra of 1-kHz bandwidth, 10-Hz frequency resolution and 600-m height resolution. Although the duty cycle is low (0.4% in the example), this capability is of particular interest for D region experiments up to 95 or 100 km, after which the spectra become too wide [*Harper*, 1978].

2.2.5. Power. The power, or power profile, mode is used for measurements of backscattered power versus height throughout the ionosphere, with an emphasis on high range resolution. The standard configuration takes measurements from 60 to 575 km in range using a 13-bit Barker code with 4-μs bauds to make up a 52-μs pulse having 600 m range resolution, although the parameters are user-configurable to produce a minimum 150-m range resolution. The default pulse repetition period is 10 ms, resulting in a 0.52% duty cycle. A 10-s average can produce an electron density profile accurate to within a few percent. An 88-baud code is also available [*Kerdock et al.*, 1986] and has been used with a baud length of 1 μs also with a 10-ms PRP and 10-s averaging [*Mathews et al.*, 1997*b*].

A coherent interference detection technique, in which pulse-to-pulse spectra are computed in real time for the lowest 77 km of range coverage, can be used during power profile measurements [*Zhou and Mathews*, 1994]. A variety of additional techniques for removing unwanted clutter and interference from power profile and other data taking modes are also being developed [*Zhou et al.*, 1999*b*]. Sources of unwanted signals include transmissions from radar and communications systems and scatter from meteors, buildings, planes, ships, and even ocean waves. Many of these signals are received in the antenna sidelobes and, owing to the geographic distance of the sources from the observatory, are prominent in lower ionospheric measurements.

2.2.6. Raw data. The preceding five modes incorporate real-time data processing programs to integrate the data and transform it to a useful form before writing on tape. Besides the convenience of data reduced at least in part online, this has the advantage of reducing the output data rates from hundreds to just a few kilobytes per second.

However, some experiments require capabilities or configurations not incorporated into the five modes discussed above, and the raw data mode is intended for use in these situations. The only limitations on this mode are the physical capabilities of the radar and data-taking systems. Significant limitations due to the

transmitter include a minimum 1-μs full power pulse or phase-coded baud, a minimum 700-μs pulse repetition period, and a 6% maximum RF duty cycle; those due to the receiving system include the $\pm$7.5 MHz bandwidth of the line feed and $\pm$15 MHz bandwidth of the Gregorian feed mentioned earlier, a maximum 12-bit A/D conversion, a maximum complex sampling rate of 10 MHz, and a maximum data rate per tape drive of 400 kbytes/s.

The features of any of the previous five modes, as well as of many other conceivable modes, can be reproduced using the raw data mode. This is true, for example, for the multipulse technique [*Farley*, 1972], the chirp technique [*Hagfors*, 1982], the alternating code technique [*Lehtinen and Häggström*, 1987], and the aliased multipulse technique [*Kohl and Rietveld*, 1996]. However, custom plotting routines must be used for real-time display of raw data mode results.

In some cases an existing mode can be modified to perform a slightly different function; the MRACF mode, for example, can be used to transmit and process standard long pulses for measuring ion or plasma line spectra. Note that the multiple transmitted frequencies normally used by MRACF cannot be "dialed in" but are achieved through the use of special transmitter phase codes [*Sulzer*, 1986*a*].

2.3. The 46.8-MHz Coherent Scatter Radar

The Arecibo 46.8-MHz coherent scatter radar was installed on the platform inside the 430-MHz carriage house in 1985 [*Röttger et al.*, 1986]. The original feed was mounted 2.16° offset from that of the 430 MHz radar but was replaced in 1986 by one allowing colinear observations (R. W. Sisk, private communication, 1997). This radar was designed for use in the MST region [*Röttger et al.*, 1981, 1986; *Rastogi et al.*, 1988] and during HF ionospheric interaction experiments [*Fejer et al.*, 1983]. It has been used for observations of thunderstorms [*Holden et al.*, 1986; *Chilson et al.*, 1993], and although the peak power is only 35 kW, when combined with the 305 m dish it is one of the most sensitive systems in the world for meteor observations at VHF frequencies [*Zhou et al.*, 1998]. The minimum and maximum full power pulse lengths are 2 and 200 μs, respectively, and the maximum RF duty cycle is 2%.

The radar is controlled by the same system used for the 430-MHz ISR, and the same data-taking modes may be used. Most commonly used are the power and raw data modes; topside and MRACF are not appropriate for this radar as the transmitted power is too low for detection of incoherent backscatter.

2.4. The 1.95-MHz Partial Reflection Radar

In 1989 the observatory acquired a 1.95-MHz medium frequency (MF) radar from the University of Adelaide, Australia, for performing partial reflection spaced antenna drift observations of winds, tides, and planetary waves between 60 and 100 km altitude [*Reid*, 1988; *Vincent and Lesicar*, 1991; *Hines et al.*, 1993; *Sürücü et al.*, 1995; *Palo et al.*, 1997]. It is located 40 km WNW of the main observatory site where it is maintained and operated in collaboration with the University of Puerto Rico at Mayagüez.

The MF radar was overhauled in 1995, and in September 1998 the data aquisition system was upgraded from 8- to 12-bit sampling and the capability was added for remotely controlled operation via the Internet. The transmitter typically operates at 25 kW peak power, using 27-μs uncoded pulses for a range resolution of $\sim$4 km. During daylight hours the radar is operated with a 12.5-ms pulse repetition period transmitting in *O* mode and recording data from 60 to 100 km. During the nighttime, the pulse repetition period is changed to 25 ms, *X* mode is used, and data are recorded from 70 to 100 km. The transmitting antenna consists of four half-wave dipoles arranged in a square array, on three sides of which are located three smaller crossed-dipole receiving antennas.

The MF system is currently being used to study the long-term dynamics of the mesosphere, specifically the effects of seasonal and other geophysical changes on mesospheric tides. The results will be compared with the incoherent scatter data taken by the 430-MHz radar and with satellite experiments such as the Upper Atmospheric Research Satellite (UARS) and the Thermosphere-Ionosphere-Mesosphere Energetics and Dynamics satellite (TIMED). The work complements observations performed at other MF sites worldwide and thus helps to provide wide geographic coverage of tidal and planetary wave activity [*Zhou et al.*, 2000].

2.5. The Digital Ionosonde

In 1997 the observatory installed a new digital ionosonde of the type known as the Canadian Advanced Digital Ionosonde (CADI) [*MacDougall et al.*, 1997]. This instrument operates from 1 to 20 MHz at vertical incidence and covers the altitude range between 90 and 500 km. Transmitter power is 600 W, 40 pulses per second are normally transmitted (20 is also possible), and either an unmodulated 40-μs pulse or a 40-μs baud, 13-bit Barker coded pulse may be used; the Barker code gives an 11-dB improvement in the signal-to-noise ratio but limits the lowest height from which echoes maybe obtained.

The ionosonde antenna is a dual orthogonal log periodic dipole array supported by a 30-m tower and providing 6 dB of vertical gain. One of the dual antennas is used for transmitting and the other for receiving. Although the Arecibo system currently has one receiver, up to four independent receivers may be used. The sampling rate is 20 μs and the altitude resolution is 6 km. Received pulses may be coherently averaged to give an additional increase in the signal-to-noise ratio proportional to the number of pulses averaged, and FFT

processing may be used to remove the linear portion of the phase drift when the ionosphere is sufficiently nonstationary that phase coherence would otherwise be lost during averaging.

The Arecibo ionosonde is primarily a middle ionosphere instrument used to calibrate the incoherent scatter radar and to observe natural and artificial spread F. Other possible uses include long-term studies of electron density variations, measurement of electron-to-ion temperature ratios, and Faraday rotation estimates in support of radio astronomy observations.

2.6. World Day

World day is the commonly used generic name for those observations which are jointly performed at upper atmospheric observatories, and in particular at incoherent scatter radar facilities, around the world. The radars include the four facilities of the American latitudinal chain, Søndrestrøm in Greenland, Millstone Hill in Massachusetts, Arecibo in Puerto Rico, and Jicamarca in Peru; the European Incoherent Scatter (EISCAT) Svalbard Radar in the Arctic Ocean and the two mainland EISCAT radars in northern Scandinavia; Kharkov in Ukraine; Irkutsk in Russia; and MU in Japan. In addition, it is hoped that a new American radar will be constructed in the near future.

World day incoherent scatter observations focus exclusively on ion line data due to the strong signal, predictable frequency, and well-developed and tested theoretical underpinning. At Arecibo the objectives of the various world day observations have in the past been met through the use of different combinations of ion line topside, MRACF, coded long pulse, and power profile measurements, all of which, as noted above, can be used to derive a wealth of geophysical parameters. For future observations it has been decided to standardize on the concurrent use of all four of these modes in a configuration which takes maximum advantage of Arecibo's ability not only to measure the E region and middle F region but also the D region and topside F region [*Zhou et al.*, 1997*c*]. Barker-coded power profiles will cover ranges between 60 and 575 km at 600-m resolution, coded long pulse will provide ion line spectra every 1.2 km between 90 and 220 km, MRACF will cover 140 to 680 km at 38-km resolution, and topside will cover 255 to 2600 km at 38-km or coarser height resolution. When using the standard 10-s run interval per program, the time resolution of the interleaved data is then just 40 s. Although including more measurements than in the past, this time resolution matches or betters that of preupgrade measurements due to improvements in the speed of the control and on-line processing computers. Other combinations of these modes may be used for specialized world day observing programs.

The importance of world day coordinated radar chain observations to the Arecibo atmospheric sciences program can be seen via an examination of the 1997 International Geophysical Calendar, which details the international schedule of coordinated atmospheric observations [*International Space Environment Service*, 1996]. At Arecibo, such coordinated observations take up ~500 observing hours per year, or about one third of the total observing time normally used by atmospheric science. Significant publications based on Arecibo MRACF world day data include *Burnside et al.* [1991*a*, *b*] and the many references cited therein. More recently, work has focused on data taken during the January 1993 ten-day world day campaign (see special sections "Aeronomy of the Solstice Thermosphere/Ionosphere System, Part 1" in *Journal of Geophysical Research*, *102*(A4), 7249-7397, 1997 and sections "Aeronomy of the Solstice Thermosphere/Ionosphere System, Part 2" in *Journal of Geophysical Research*, *102*(A6), 11,475-11,555, 1997).

In order to obtain vector ion drift and thermospheric neutral wind velocities, world day observations at Arecibo often involve scanning, in which the zenith angle is fixed at 15° and the azimuth is varied in a predetermined pattern [*Burnside et al.*, 1987]. In the past, the 16 min required to complete a 360-degree scan in azimuth set the maximum time resolution for single beam observations of three-dimensional (3-D) vector velocities, with 8 min required for a 2-D coplanar observation. When two-beam ISR capability becomes available, 3-D velocities will be measured in 8 min, and a single 10- or 20-s integration will provide a coplanar 2-D vector measurement. Thus dual-beam operation will allow for simultaneous measurements of north-south drifts parallel and perpendicular to the geomagnetic field, although scanning will still be required to measure the east-west velocity component. The availability of instantaneous information concerning the presence and development of spatial inhomogeneities in the plane of the beams will be a qualitatively new capability of dual-beam observations.

As discussed in section 2.2.2, the high signal-to-noise ratio available from Arecibo middle F region observations means that the division of transmitted power into two beams will provide the advantage of an additional channel of information with essentially no degradation in quality of the resulting signals. It should also be noted that owing to the great sensitivity of the Arecibo dish, accurate horizontal drift velocity measurements are possible in spite of the small horizontal component seen when using a 15° zenith angle. (The maximum possible angle of 20° is not used for the vector measurements because of the decline in signal-to-noise which occurs due to spillover of the feed pattern past the edge of the main dish at the largest zenith angles.) The net effect produces an advantage for Arecibo horizontal drift observations since the volume from which orthogonal samples are obtained is much less than when larger angles are used. A recent view of the Arecibo feed platform with the line feed and the new Gregorian feed is shown in Plate 1.

2.7. Ion Line Observations

In this section we present recent results from Arecibo 430-MHz ion line observations.

2.7.1. Vertical ion velocities. One result of the 1993 ten-day world day campaign is illustrated by *Zhou and Sulzer* [1997, Figure 4a], who show vertical ion velocities during quiet winter conditions possessing a large downward component throughout the entire day and averaging 20 m/s near the F region peak. The downward ion drift can be seen to be due mainly to the northward drift along the downgoing geomagnetic field line. Plate 2 presents average vertical drift versus time of day, altitude, and season, clearly showing the winter daytime effect and underscoring the time and seasonal dependence of the ion velocities. The data were taken using the MRACF mode.

2.7.2. Ion composition and temperatures. Owing to the additional time made available for analysis, the upgrade has yielded improvements not only in hardware but also in Arecibo data processing capabilities. It is now possible to determine the concentrations of oxygen, helium, and hydrogen ions in the topside ionosphere between the F region peak and 2000 km with 10-min time resolution. Observations show that a layer of He^+ can exist at altitudes as low as 500 km with concentrations >10% during solar minimum equinox conditions [*González and Sulzer*, 1996] and at concentrations of 30–40% and as high as 60% near 800 km during the very early morning at solar maximum [*Erickson and Swartz*, 1994; *S. A. González et al.*, Variations in the topside helium ion concentrations over Arecibo between October 1988 and October 1995, manuscript in preparation, 2000].

These same data processing improvements have allowed the simultaneous measurement of oxygen ion, proton, and electron temperatures (T_{O+}, T_{H+}, and T_e). *Sulzer and González* [1996] show the dramatic variation in these temperatures over the course of a day; the data for these observations were taken using the topside mode described above, which, as noted above, has now been incorporated into the standard Arecibo world day program.

2.7.3. The impulse response of the ionosphere. The total solar eclipse of February 1998 presented a unique opportunity for studying the ionospheric impulse response to the lunar shadow. At ground level the umbra was 92 km in diameter and passed just 400 km south of Puerto Rico, producing a brief local nightfall simultaneously at all altitudes. The Sun as seen from Arecibo was 90% and 87% eclipsed on the ground and at 300 km altitude, respectively, and the radar was pointed vertically. Incoherent scatter ion line observations were performed using the topside mode with a 10-ms pulse repetition period and with range gates extending from below 200 km to over 2000 in altitude. A 300-μs pulse was transmitted, shorter than that used in the standard world day mode in order to improve height resolution in the F region. Ion line power profile and coded long pulse plasma line data were also recorded. As can be seen in Plate 3, which contains the hydrogen ion fraction derived from the topside data, eclipse-driven recombination and transport effects occurred as expected (*B. MacPherson et al.*, The effects of the February 26, 1998 solar eclipse on the $O^+ - H^+$ transition altitude over Arecibo, manuscript in preparation, 2000). The strong gradients produced by the passing shadow are expected to have launched gravity waves in the thermosphere. Data from simultaneously recorded ion line power profiles and coded long pulse plasma line spectral measurements, similar to those described in more detail in section 2.8 below, will be used to test this hypothesis.

2.7.4. Planetary waves. Quasi 2-day planetary waves have been studied using data from ISR 4-μs baud ion line power profiles obtained during the January 1993 ten-day run. Planetary waves are particularly prominant at tropical latitudes, and this, along with the fact that the Arecibo ISR can observe these waves between 100 and 170 km where other ground-based instruments such as MF and meteor radars and ionosondes cannot, makes Arecibo ideal for studying planetary wave activity in the lower thermosphere [*CEDAR Science Steering Committee*, 1997; *Altadill and Apostolov*, 1998]. For example, the January 1993 data show quasi 2-day planetary wave penetration to an altitude of at least 145 km along with a large effect on the ionosphere below 95 km [*Zhou et al.*, 1997*b*]. Figure 2 shows a consistent 2-day modulation in the electron density during the period of January 21–28, 1993, consistent with the 2-day components in the neutral wind. *Zhou et al.* [1997*b*] have also used wind and temperature data derived from coded long pulse ion line observations performed during January 1997 to study tidal structure in the lower thermosphere between 95 and 145 km. They found that planetary waves and 6- or 8-hour tides can compete with the diurnal and semidiurnal tides, which were expected to dominate the data. Similar data have been compared with results from the Thermosphere-Ionosphere-Mesosphere Electrodynamcs General Circulation Model (TIME-GCM) [*CEDAR Science Steering Committee*, 1997; *Zhou et al.*, 1997*b*].

2.7.5. Ion rain. High-resolution (150 m, 10 s) ion line power profile data can be used to study layering phenomena in the E region and their connection to the F region [*Mathews*, 1998]. Perhaps the most intriguing new result of this work is the discovery of the phenomenon known as ion rain [*Mathews et al.*, 1997*b*], an example of which is given in Figure 3. Ion rain has been observed to occur in the evening before midnight local time in the height range spanning the lower E region to the lower F region. It is known to be is associated with intermediate layers [*Fujitaka and Tohmatsu*, 1973]. While descending from the F region, these layers may be modified by large oscillations having ~10 km vertical

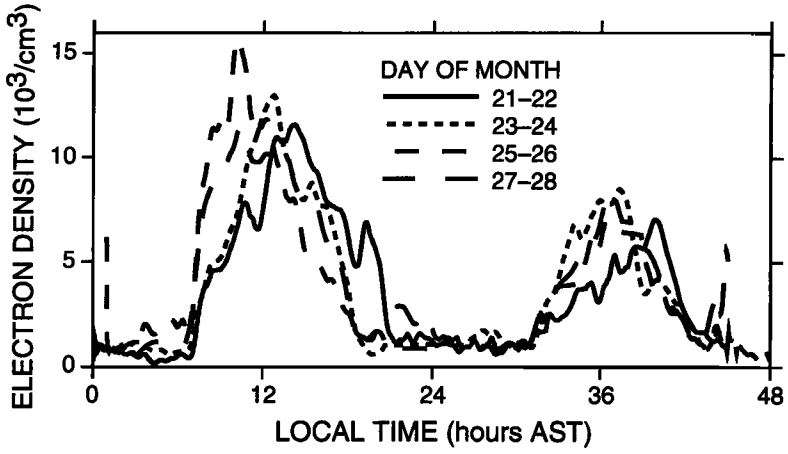

Figure 2. A quasi 2-day planetary wave observed via its modulation of the electron density between 89.8 and 92.2 km altitude during January 21–28, 1993; the data are overlaid in 48-hour blocks in order to more clearly show the 2-day period. Arecibo is well suited for studying planetary wave penetration into the thermosphere due to its location at tropical latitudes, where such waves are prevalent, combined with the ability of the 430-MHz ISR to observe these waves between 100 km and 170 km, where other ground-based instruments cannot. Adapted from *Zhou* [1998].

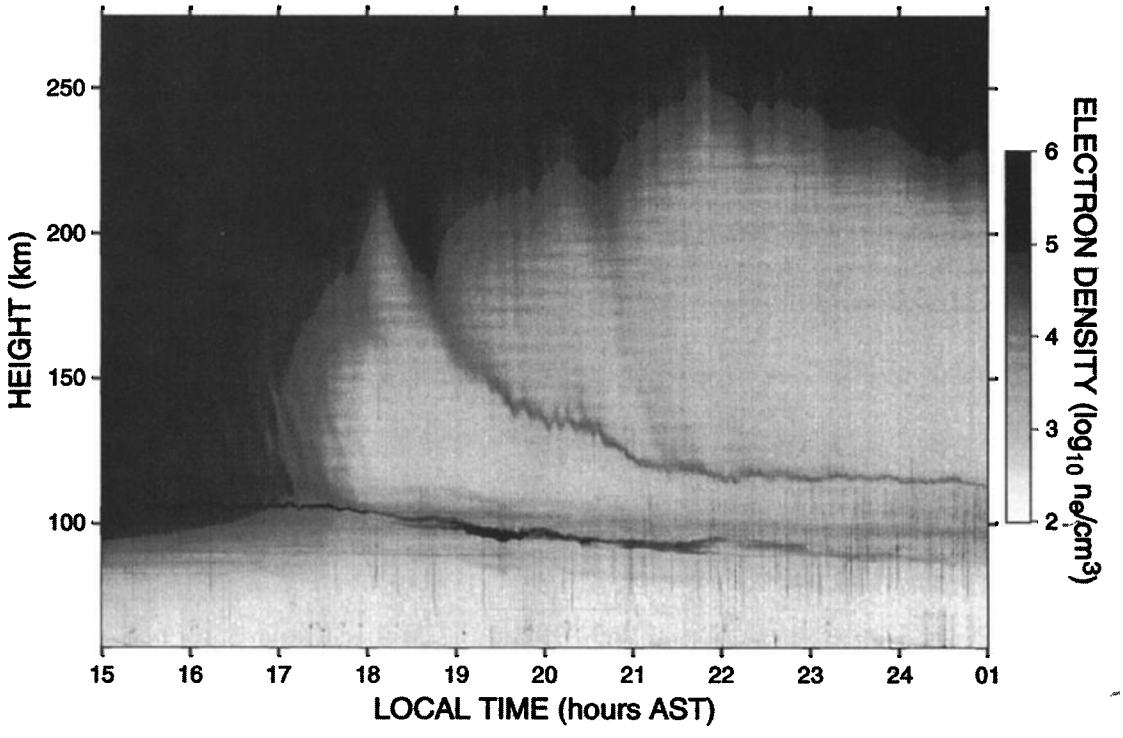

Figure 3. A height versus time plot showing the variation in the electron density between 60 and 270 km on September 2, 1994. An intermediate layer is seen descending from the base of the F region at 1830 LT, and ion rain is clearly visible between 1900 and 2200 LT merging with the downgoing oscillations of the intermediate layer. The layer descending from 110 to 85 km is sporadic E; the light vertical steaks occurring mainly between 80 and 110 km altitude are meteor echoes broadened by unsuccessful decoding to twice the length of the radar code. The structure and dynamics of the ion rain and of the layers varies greatly from day to day; the detailed explanation of the variability is another topic of current interest. The data were taken using an 88-baud code with 1-μs baud length and 10-ms pulse repetition period [*Mathews et al.*, 1997*b*].

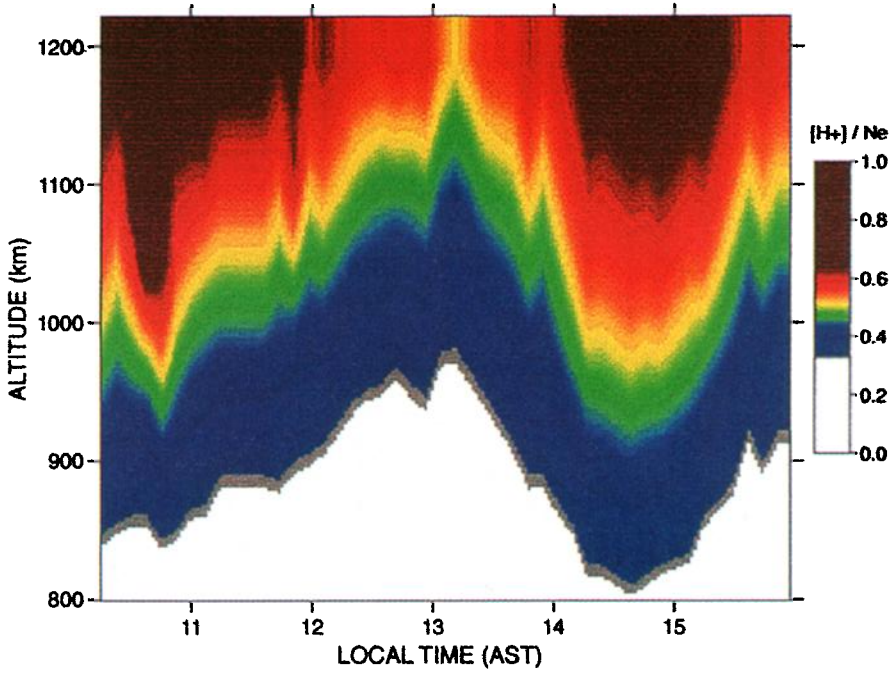

Plate 3. Arecibo ISR data taken during the total solar eclipse of February 26, 1998, showing the measured proton fraction ($[H^+]/n_e$). The signature of the lunar shadow can clearly be seen in the dramatic collapse of the protonosphere, with the transition height, defined as the height where $[H^+]/n_e = 0.50$, falling from 1100 km to about 950 km between 1300 and 1500 LT. This collapse is due in large part to the decline in the photoelectron flux and subsequent cooling of the ionosphere, which occurred during the eclipse, and the subsequent recombination and transport effects (*B. MacPherson et al.*, The effects of the February 26, 1998 solar eclipse on the $O^+ - H^+$ transition altitude over Arecibo, manuscript in preparation, 2000). The sensitivity of the measurement is somewhat lower than usual, as the topside mode was used with a shorter than normal transmitter pulse for improved height resolution in the F region and due to the adverse consequences of interference from nearby radar transmissions within the Arecibo incoherent scatter band. The passing shadow is expected to have generated gravity waves, which are being investigated using simultaneously measured ion line power profiles and coded long pulse plasma line spectra.

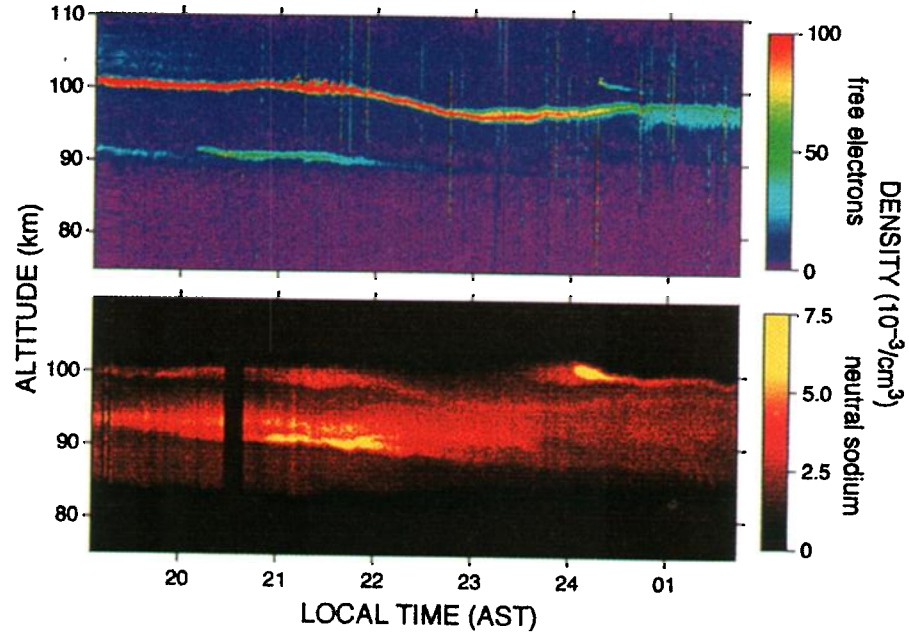

Plate 4. Dynamics of lower E region layers over Puerto Rico on March 2, 1998, as seen via Arecibo measurements of 430-MHz radar incoherent backscatter from free electrons and 5890-Å lidar resonance fluorescence backscatter from neutral sodium [*Friedman et al.*, 2000]. The radar data were taken using an 88-baud code with 1-μs baud length and 10-ms pulse repetition period [*Mathews et al.*, 1997*b*]; the lidar had a 40-ms pulse repetition period with a 10-ns pulse which was integrated into 0.25-μs range bins. The measurements thus have range resolutions of 150 and 37.5 m, respectively. The time resolutions as determined by the temporal integration periods are 10 s for the radar and 30 s for the lidar data. These measurements were taken during the NASA Coqui II rocket campaign, which took place in Puerto Rico in February, March , and April 1998.

amplitude and an apparent duration of ~12 min, and ion rain may then appear as rapidly downward moving streaks of ionization which converge with the intermediate layer exclusively on the downward side of the oscillations. *Mathews et al.* [1997*b*] suggest that ion rain may be related to short horizontal-scale electric fields possibly originating from Perkins-like instabilities in the base of the F region.

2.8. Plasma Line Observations

At Arecibo, coded long pulse plasma line measurements can be used to determine the plasma frequency and electron density to 1 part in 1000 in ~2 s; this is orders of magnitude more accurate and rapid than is possible when using ion line measurements. At this accuracy, density perturbations due to gravity waves propagating upward into the ionosphere from the mesosphere (with downward phase velocity) can be easily observed [*Djuth et al.*, 1997*b*]. The narrow bandwidth of the 430-MHz line feed currently makes plasma line observations difficult at the F region peak itself, but the upgraded radar will no longer suffer this limitation.

2.8.1. Langmuir equation and field aligned currents. Coded long pulse data are being used to investigate corrections to the standard Langmuir wave dispersion equation which, when finalized, will allow calculation of the bulk electron drift velocity from the plasma line Doppler shift (up versus down), thus giving, along with ion drift, a measurement of field-aligned current. Such currents are thought to occur during disturbed conditions at Arecibo [*Behnke and Harper*, 1973; *Muldrew*, 1980; *Zhou and Sulzer*, 1997]. Figure 4 shows two profiles of the difference between the upshifted and downshifted plasma line frequencies versus height, along with a calculation of the difference frequency computed from a modified version of the Langmuir wave dispersion equation which includes a nonisotropic heat flow term [*Kofman et al.*, 1993]. The electron temperatures and temperature gradients required for the calculation were obtained from simultaneously measured MRACF ion line data. Although preliminary, the results appear

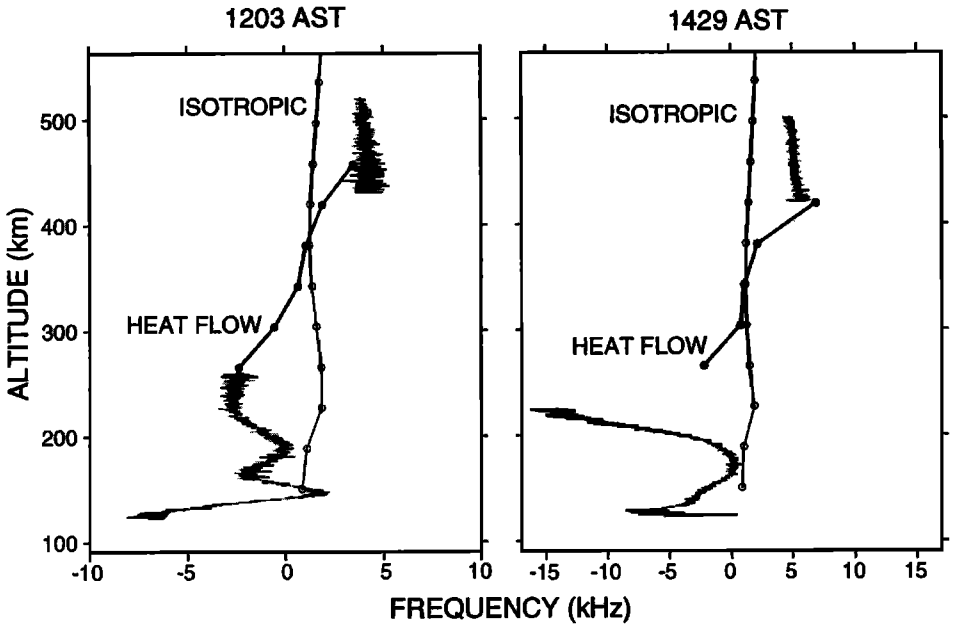

Figure 4. The frequency difference between the upshifted and downshifted plasma line frequencies on July 1, 1993, as measured using the coded long pulse technique (jagged shaded curve) and as computed from the isotropic Langmuir dispersion equation (open circles) and from a nonisotropic Langmuir equation incorporating a heat flow correction formulated by *Kofman et al.* [1993] (solid circles). The circles give the altitudes at which the electron temperature and temperature gradient required for the calculation were computed from incoherent scatter ion line data measured using the MRACF radar mode. The gap in the plasma line data between about 250 and 430 km occurred when the plasma line frequencies around the F region peak exceeded the relatively narrow bandwidth of the 430-MHz line feed. Note that the nonisotropic (heat flow) dispersion relation appears to bridge the gap from the bottom to topside F region much better than the traditional isotropic theory. The theory cannot be compared with the measurements below 250 km due to the relatively rapid change in parameter values in that region as compared with the resolution of the MRACF data, and above ~450 km the assumptions necessary for the validity of the heat flow correction are no longer valid. The measurements were made during quiet conditions, and field-aligned drifts and currents have been assumed to be negligible. When this technique has been perfected, measurements performed during disturbed conditions may be used to measure field-aligned currents of 10 $\mu A/m^2$ from incoherent scatter measurements alone.

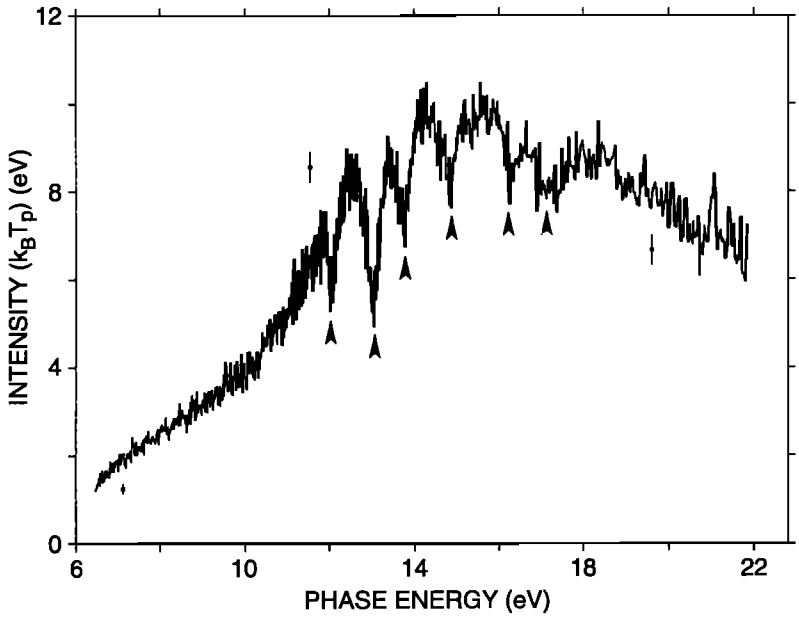

Figure 5. Plasma line intensity versus Langmuir wave phase energy derived from coded long pulse observations of the plasma line spectrum versus altitude in the bottomside F region, May 15, 1991, 1324:00–1326:48 LT. The lowest and highest energies shown (~6 and ~22 eV) correspond to data taken at altitudes of 125 and 275 km, respectively. Three representative 1σ error bars are also shown. Plasma line intensity is directly related to the intensity of the photoelectron flux, and the dips in the energy spectrum (marked by the arrowheads) are believed to be caused by inelastic collisions between photoelectrons and neutrals. Adapted from *Djuth et al.* [1994].

promising. When the method is perfected, it will be possible to measure currents of 10 $\mu A/m^2$ with a time resolution of 15 seconds [*Showen*, 1979; *Djuth et al.*, 1997*b*].

2.8.2. Collisional damping of the photoelectron intensity spectrum. The coded long pulse technique can also be used to observe the plasma line intensity with fine altitude resolution. As shown in Figure 5, since the plasma line frequency varies with height, a plot can be made of the plasma line amplitude spectrum versus frequency or, equivalently, the photoelectron intensity spectrum versus energy [*Djuth et al.*, 1994]. The dips in the energy spectrum are believed to be caused by inelastic electron-neutral collisions. These measurements take full advantage of the sensitivity of the Arecibo radar, and the data have 100 times better energy resolution and 10 times better temporal resolution than previous measurements of this kind.

2.9. Meteor observations

Incoherent scatter radars have been used for observations of meteors since the initial observations by Evans [1965, 1966] at Millstone Hill. Recently, work has been carried out at Jicamarca [*Chapin and Kudeki*, 1994], EISCAT [*Pellinen-Wannberg and Wannberg*, 1994], and Arecibo [*Zhou et al.*, 1995]. Meteor observations at Arecibo have typically used 1- to 8-μs uncoded transmitter pulses in the raw data mode discussed above. Pulse repetition periods have typically been between 5 and 1 ms, decreasing as the maximum rate for data recording has increased. A pulse repetition period of 1 ms is sufficient for recording data free from height aliasing effects out to 150 km in range, thus including all of the meteor ablation zone. Figure 6 gives an example in which the 430- and 46.8-MHz radars are used simultaneously and shows the power versus time and height format in which the data are typically viewed.

The meteor echoes seen with the 430-MHz system have measured radar cross sections as low as 3×10^{-8} m^2 and in some cases even less. Depending on the particular assumptions made regarding the meteor scattering mechanism, the corresponding electron line density is of the order of 4×10^{9} m^{-1}. The visual magnitude of these meteors may be estimated by comparing the detection rates with rates from optical observations. The result is a calculated magnitude of approximately +16, which in turn corresponds to an estimated meteoroid mass of about 10^{-6} g [*Mathews et al.*, 1997*a*]. The meteors seen by the Arecibo 430-MHz radar are thus among the faintest observed by any type of ground-based instrument.

The example of Figure 6 is typical of many of the meteors observed by both the 430-MHz and 46.8-MHz radars in that the long lifetime of the backscattered signal indicates that the primary echoes originate from objects traveling in the radial direction of the narrow antenna beam [*Zhou et al.*, 1998]. These echoes cannot be explained by theories which assume perpendicular

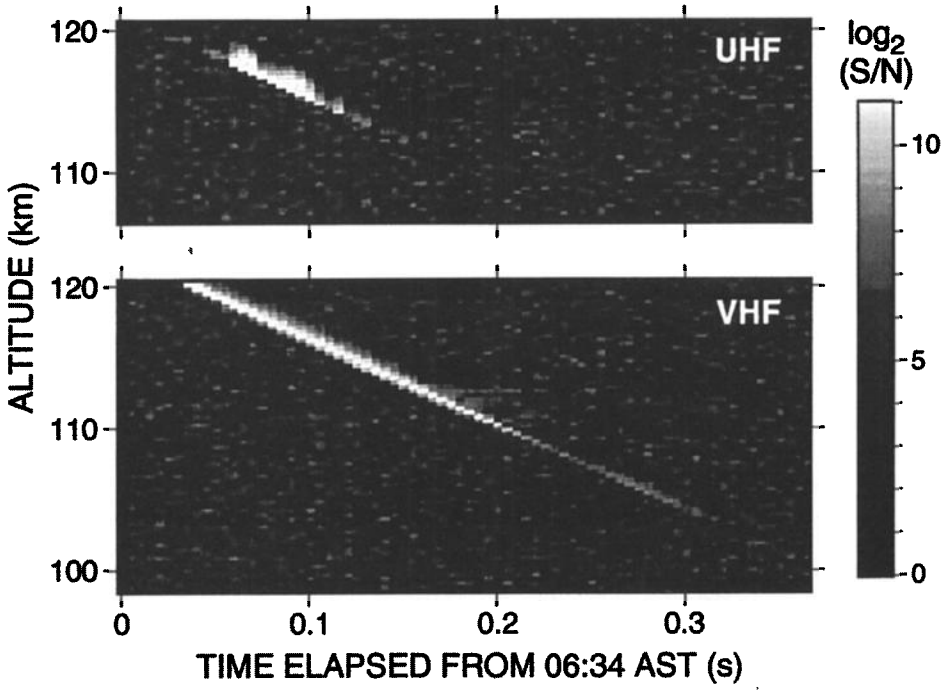

Figure 6. A power versus time and height plot of a meteor observed simultaneously with the Arecibo 430- and 46.8-MHz radars on September 30, 1994, near 0600 LT using a 2-μs uncoded pulse and 5-ms pulse repetition period on each system with no integration. The upper range limit at 120 km was determined by the capacity of the data-taking system to record raw data samples. This example is typical of many of the meteors observed by the Arecibo radars in that the long lifetime of the backscattered signal indicates that the primary echoes originate from objects traveling in the radial direction of the narrow antenna beam and that their orbits may thus be determined using these data alone. The meteors seen by the Arecibo 430-MHz radar are among the faintest observed by any type of ground-based instrument. Adapted from *Zhou et al.* [1998].

scatter from the trail. Explaining the scattering mechanism is the most important theoretical question posed by these observations.

The fact that many of the meteors observed at Arecibo fall directly into the radar beam means that their orbits may be determined using these data alone. On the basis of the orbital information thus derived, *Mathews et al.* [1997*a*] suggest that micrometeors pervade the inner solar system and may be primordial in origin. These data are also being used to determine the flux of extrasolar system dust particles.

Simultaneous radar, lidar, and passive optical observations, such as those made at Arecibo during the 1997 and 1998 Leonid meteor showers, may shed light on a number of aeronomy problems, such as meteoric effects on mesopause chemistry and on the formation of sporadic E and sporadic metal layers [*Zhou et al.*, 1999*a*].

3. Optical Instrumentation and Observations

The Arecibo optical program includes both passive airglow and active lidar observational capabilities, both of which can be used for observations of the ionosphere. The passive instruments include two modular Fabry-Perot interferometers, an Ebert-Fastie spectrometer, and four dual-channel tilting filter photometers. The detectors, which are GaAs photocathode photomultiplier tubes with 10% or greater quantum efficiency and gains of 10^6, permit observations between 3000 and 9000 Å. These instruments are housed in the original Arecibo optics building, where six plexiglas domes and four dual-axis 0.1° per step programmable mirror systems are available for use. The active instruments, housed in the new optics laboratory, include a Doppler Rayleigh lidar and two resonance fluorescence lidars, all using photomultiplier detectors similar to those used by the passive Arecibo instruments. The passive instruments are capable of automatic operation. Visiting instruments are also common at Arecibo, and one or two are typically installed on site at any given time. Arecibo optical observations are currently limited to nighttime and twilight measurements [*Tepley*, 1989]. The instruments and some of the ionospheric observations made with them are described in more detail in sections 3.1-3.6.

3.1. Airglow instruments

3.1.1. Fabry-Perot interferometers. Arecibo's two Fabry-Perot interferometers are used to measure the nighttime neutral wind and temperature from the Doppler shift and broadening of F region O(^1D) 6300

Å red line emissions from around 300 km and E region O(^1S) 5577 Å green line emissions, respectively, originating near 100 km altitude [*Ingham*, 1972]. Thermospheric and exospheric 6563 Å H_α emissions are also observed. The wind velocity and first-order velocity gradient are obtained by alternating observations between zenith and eight equally spaced azimuth angles at a elevation angle of 30°. The interferometers are designed for narrow bandwidth observations; the bandwidth used for 6300 Å observations is 0.02 Å with a 0.2 Å free spectral range; at 6563 Å the bandwidth is normally 0.08 Å. The instruments have 0.15-m clear apertures and 1.2-m focal lengths. The field of view is typically 0.25° in diameter, and the spectral line sensitivity is two counts per second per rayleigh. Integration times are typically 20 s per point; with seven points per spectrum and nine spatial positions, so that one observation takes ~20 min. Temperature can typically be measured at 6300 Å to within 50 K and velocity to within 20 m/s; at 5577 Å the corresponding values are 5 K and 20 m/s. The two etalons may be combined for very high resolution measurements.

3.1.2. Ebert-Fastie spectrometer. The spectrometer used at Arecibo is of the Ebert-Fastie configuration with 0.15-m-long entrance and exit slits and a focal length of 1 m. This instrument can be used to scan rapidly over a broad frequency range and is most often used to measure line intensities within molecular rotational spectral bands in order to compute nighttime neutral temperatures. The most commonly observed species are OH and O_2, both of which have rotational bands throughout the 3000–9500 Å range. Of these, the most commonly observed lines are those in the 8400 Å OH (6–2) and 8645 Å O_2 (0–1) bands. The source region of the former is found near 85 km altitude, while the latter orginates near 95 km in the mesopause region, where the lowest atmospheric temperatures occur. The 7320 Å O^+ line has also been observed with this instrument during thermospheric twilight [*Meriwether et al.*, 1978]. A typical observation might take 6 min, incorporating a 240-point scan, a 0.5-s integration at each point, and a sum over three scans; the temperature obtained during such a measurement is typically accurate to within ~10 K and the intensity error is about 10%. The bandwidth is adjustable between 0.2 and 10 Å, with a maximum scanning range of 1000 Å anywhere between 3500 and 8700 Å. The Arecibo spectrometer has a rectangular field of view which is variable from 8.5° by 0. degree to 8.5° by 8.5° and a typical sensitivity at 6300 Å of 25 counts per second per rayleigh per angstrom.

3.1.3. Photometers. The four Arecibo photometers [*Eather and Reasoner*, 1969; *Herrero and Meriwether*, 1980] are used to monitor the airglow intensity using either a two-point on-line/off-line measurement or by scanning in frequency over the emission region; they may also be used in pairs to measure rotational temperature. About 10 s is required per data point, or 20 s for a complete measurement, providing neutral temperatures accurate to ~3–5 K and with an intensity error of ~5% [*Tepley et al.*, 1981]. Spectral information is obtained by varying the tilt of a narrowband interference filter; several filters are available for airglow emissions throughout the visible portion of the spectrum. The tilt range is 10°, resulting in a ~25 Å scan. The resolution of these instruments ranges between 3 and 10 Å, depending on the filter used; the field of view diameters are adjustable between 0.25° and 5.0°, and their sensitivity is typically ~300 counts per second per rayleigh per angstrom. The relatively high sensitivity of photometers allows them to be used for observing rapid changes in airglow intensity on a timescale, depending on the observed intensities, of 1 s to several seconds. As a result, they are often used to provide background intensity calibration measurements in support of Fabry-Perot interferometer observations. The photometers themselves are calibrated using a ^{14}C source.

3.2. Lidars

Optical instrumentation for active observations in the ionosphere currently consists of pulsed dye and Alexandrite ring laser systems intended for resonance fluorescence lidar observations of naturally occurring atomic metal layers between roughly 80 and 105 km [*Measures*, 1984; *Beatty et al.*, 1989; *Castleberg*, 1997] and of a frequency-doubled Nd:YAG laser for Doppler Rayleigh lidar measurements of neutral wind, absolute temperature, and relative density from 20 to 60, 25 to 60, and 25 to 70 km in altitude, respectively [*Measures*, 1984; *Tepley*, 1993, 1994; *Castleberg*, 1997; *Friedman et al.*, 1997].

The Nd:YAG system was acquired by the observatory in February 1990 and has been used for 5320 Å Doppler Rayleigh observations of upward coupling from the stratosphere/lower mesosphere to the mesosphere/lower thermosphere/ionosphere system; outputs at 3547 Å and 10640 Å are also available. The Alexandrite ring laser system [*von Zahn and Höffner*, 1996] arrived in late 1995 and saw first light in May 1996 [*Castleberg*, 1997]. It has its fundamental frequency band between 7200 and 8000 Å and is currently used for observations of neutral potassium layers at 7699 Å. The system has a sufficiently narrow emission bandwidth that these observations can be used to measure mesospheric wind and temperature; this capability is expected to become available for use in the summer of 1999. In the future, neutral iron and calcium ion layers will be observed at 3719 and 3934 Å, respectively, using the 3600–4000 Å second harmonic frequency band. A frequency source, in the form of a low-power seed laser, is required for each operational frequency. The Alexandrite system has also been used to measure the neutral temperature from 7699 Å Rayleigh scattering between 25 and 70 km and, after two levels of frequency conversion, to measure neutral sodium at 5890 Å between 80 and 105 km (although this is not practical for routine

measurements); along with the Nd:YAG system it has been used to observe Mie scattering from aerosols in the upper troposphere and lower stratosphere at 3850, 5320, and 7699 Å [*Castleberg*, 1997]. The pulsed dye laser system was acquired for the Coqui II campaign of early 1998 (described in section 5.1). It arrived in December 1996 and saw first light in May 1997. The dye laser must be pumped in order to operate, a job for which the Nd:YAG laser is used; it is intended primarily for 5890-Å neutral sodium layer density measurements [*She and Yu*, 1994] and in the future will also be used for 4227-Å neutral calcium observations.

Transmissions occur through open ports in the laboratory ceiling. The dye system transmits a 10-ns pulse every 25 ms at 7.5 MW peak (3-W average) power, the Alexandrite system transmits a 200-ns pulse every 50 ms at 1 MW peak (4-W average) power, and the Nd:YAG system transmits a 6-ns pulse every 25 ms at 66 MW peak (16-W average) power. All three lidars use 0.80-m-diameter Cassagrain telescopes, located on the roof of the lidar laboratory, for receiving; the power-aperture products are 1.4, 1.9, and 7.5 W m^2, respectively. Although the telescopes are fully steerable, the current biaxial transmit/receive geometry requires fixed pointing during observations. Coaxial transmissions, which will allow the full pointing capability to be used, will be implemented in the near future. The receiver fields of view are each 0.5 mrad, and each telescope is coupled via optical fiber to a photomultiplier tube detector. A 0.70-m focal length Fabry-Perot interferometer is available for high-frequency resolution measurements. Data may be collected with sampling as fine as 5 ns, but coarser sampling is generally used.

The resonance lidars may be used to measure metal densities with typical time and range resolutions of 30 s and 37.5 m, respectively. The minimum detectable density is determined by the power-aperture product of the lidar and the sensitivity of the photomultiplier tubes, which can respond to as few as one or two photons. For an integration period of 30 s this corresponds to a density of <10 atoms/cm^3, and with appropriate data processing <1 atom/cm^3 may be detected. Measurements of mesospheric wind and temperature with the Alexandrite system will have a time resolution of 10 min, and it is possible that the range resolution will be as good as 150 m. Velocities and temperatures will be accurate to about 10 m/s and 10 K, respectively. Measurements with the Doppler Rayleigh system typically have a time resolution of 10 min and a range resolution of 1.5 km. Wind velocities are accurate to within 10 m/s at 45 km altitude [*Friedman et al.*, 1997]; in the future this altitude will be increased to 60 km or more. Measured temperatures have a typical accuracy of 10 K at altitudes above 60 km.

3.3. Visiting Instruments

The Arecibo optical program regularly hosts visiting instruments, which generally provide observations complimentary to Arecibo's own capabilities. Recent visiting instruments have included a Fabry-Perot interferometer from Scientific Solutions of Massachusetts, a spectrometer from Arizona State, a photometer from Clemson University, and several imagers. Since imagers have not yet been discussed, a few details will be given here.

Imagers may be used to study the spatial structure of relatively slowly changing airglow emission intensities over large regions of the sky. Visiting all-sky imagers, fielded by Utah State and Boston Universities, have been used to produce images of 5577-Å oxygen and broadband OH emissions [*Taylor and Garcia*, 1995] and 6300-Å atomic oxygen emissions [*Baumgardner et al.*, 1993], respectively. A third all-sky imager has since been installed by the space plasma physics group at Cornell University and used to measure 6300-Å emissions from the F region, 5577-Å emissions from the E region, and broadband OH emissions from the mesosphere between 7150 and 9300 Å. The Cornell imager produces signal-to-noise ratios ranging from ~20 to ~50 using a 14-bit pixel depth, 1024 by 1024 pixel silicon CCD cooled to −40°C [*Garcia et al.*, 1997]; the CCD is 80% quantum efficient at visible wavelengths. Typical exposure times are 90 s for the narrowband atomic oxygen observations and 15 s for OH. This instrument has proven to be significantly more sensitive than image-intensified systems. Imagers fielded by the Air Force Research Laboratory and the Naval Research Laboratory [*Bernhardt et al.*, 1989*b*] have also been used to study HF-enhanced airglow, as discussed in section 4.1.3. Observations obtained with the Cornell device are included in the examples presented in section 3.4.3.

3.4. Observations of Atomic Oxygen in the F Region

Most 6300-Å emissions originate just below the F region peak, where maximum O_2^+ densities are found. The 6300-Å red line is produced when O_2^+ recombines with an electron, producing one or two excited atoms of atomic oxygen; a 2-eV photon is then emitted during relaxation to the ground state.

3.4.1. Postmidnight collapse. An example of Fabry-Perot interferometer and photometer data showing the postmidnight collapse of the $F2$ layer is given in Figure 7. At about 0300 LT the meridional wind, which had been blowing southward, begins to abate and shift to the north. While a southward wind tends to hold the plasma to higher altitudes, the effect of the wind reversal to the north forces the plasma down the geomagnetic field lines into regions of greater O_2^+ density. The outcome is an increase in the recombination of O_2^+, dissociating the molecule into the atomic oxygen $O(^1D)$ excited state and resulting in the large increase in 6300-Å airglow intensity observed at about 0330 LT [*Nelson and Cogger*, 1971].

3.4.2. F region gravity waves. *Mendillo et al.* [1997] gives an example of image data taken with the

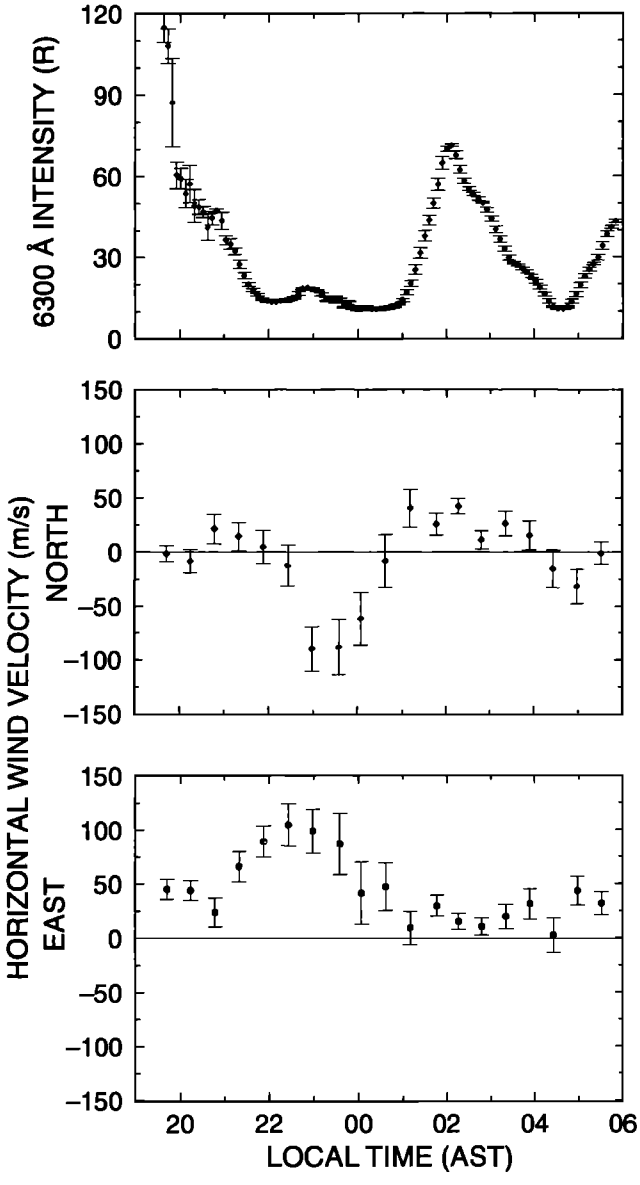

Figure 7. Arecibo 6300-Å intensity and derived neutral wind measurements showing the postmidnight shift from southward to northward thermospheric winds during the night of March 1–2,1998. This causes a decrease in the height of the F region known as the postmidnight collapse and a corresponding increase in airglow intensity due to increased recombination of O_2^+. The velocity error bars are ±1 standard deviation; note the dramatic decrease in the magnitude errors at times of strong airglow intensity. The error bars on the intensity data behave similarly; these indicate the variations of the signal within an average of 15 points, each integrated for 10 s and with a standard deviation of a few percent. The airglow intensity and spectral line Doppler shifts, from which the wind velocity data are derived, were measured with an Arecibo photometer and Fabry-Perot interferometer, respectively. Due to the overhead incurred when running several instruments simultaneously, the time resolutions are somewhat less than what is possible for each instrument alone.

Boston University instrument in which gravity wave, or buoyancy wave, signatures are seen in the hours preceding local midnight during the January 1993 ten-day world day period described in section 2.6. The wavelength was ~500 km and propagation velocity was ~100 m/s, yielding a period at zenith of ~90 min; these parameters are typical of long-period F region gravity waves. Simultaneous 430-MHz radar data show that these neutral atmospheric waves have associated electric potentials which reduce the ion drag damping experienced by the waves [*Kelley and Miller*, 1997].

3.4.3. Traveling ionospheric disturbances. Figure 8 shows a westward propagating traveling ionospheric disturbance (TID) wave packet observed at 6300 Å on January 6, 1997, using the Cornell imager. Although these structures usually travel to the southwest, westward is emphasized here since classic TIDs from the auroral oval generally track southward. This particular packet had a 30-min period, a 105-km horizontal wavelength, and a 58 m/s phase velocity. *Kelley and Miller* [1997] hypothesize that these features are related to the turbulent upwellings observed by the MU radar [*Fukao et al.*, 1991; *Kelley and Fukao*, 1991] since they have similar periodicities, phase velocities, and orientations; *Behnke* [1979] and *Miller et al.* [1997] note that the maximum growth rate for the Perkins instability [*Perkins*, 1973] is in the same direction. An exciting recent result, in which coherent echoes were detected from Puerto Rico by two 50-MHz radars (fielded by the universities of Illinois and Cornell) while the imager observed banded southwest propagating structures, appears to confirm this hypothesis (E. Kudeki et al., personal communication, 1998). The observed Doppler shift at times exceeded 300 m/s.

Perhaps even more spectacular is the image in Figure 9 from the evening of 22–23 November 1997, during which Kp reached 7 and a remarkable surge of alternating bright and dark 6300-Å airglow bands coursed poleward from the southern sky, bifurcating en route along the northern edge. One of the dark portions is seen in the left-hand side of Figure 9. The overplot, from GPS satellite 31, shows the trajectory corresponding to the plot of relative total electron content (TEC) below, also viewed from Puerto Rico. Note that the darkest airglow regions are colocated with deep TEC depressions, while the bright bands have very large TEC values. The excursion is 20 TEC units. Such a behavior is the opposite one expected from purely chemical arguments since bright airglow should come from rapidly recombining regions. Remarkably, this and subsequent structures became oriented in the same direction as those in Figure 8 and traveled in the same general direction. Such westward tracking, along with the early evening development over Arecibo, rules out an origin associated with equatorial spread F.

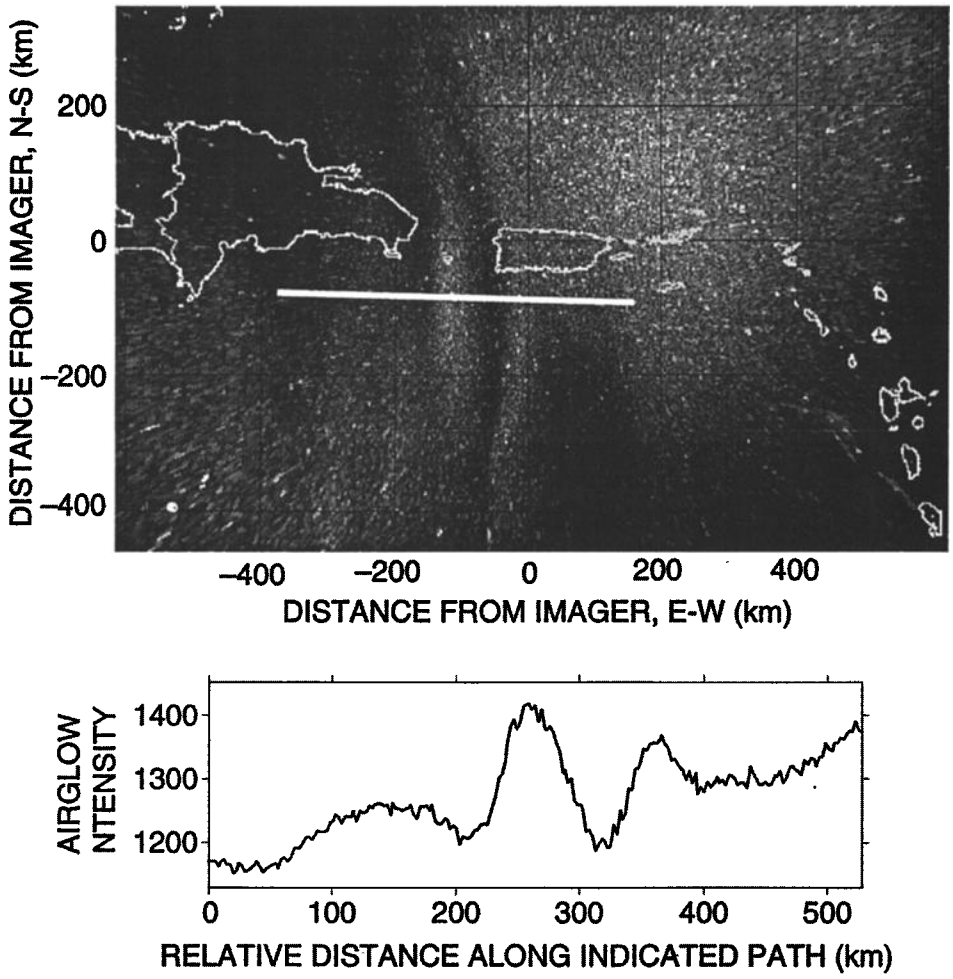

Figure 8. (top) A traveling ionospheric disturbance (TID) observed in the F region over Arecibo by a 6300-Å imager on January 6, 1997. (bottom) The percentage change in airglow luminosity along the horizontal white line located near the center of the image. Although TIDs from the auroral oval generally track southward, this structure, which had a 30-min period, 105-km horizontal wavelength, and 58 m/s phase velocity, moved westward and is hypothesized to be related to turbulent upwellings observed by the MU radar [*Fukao et al.*, 1991; *Kelley and Fukao*, 1991; *Kelley and Miller*, 1997].

3.5. Observations of H_α and Metastable He in the Thermosphere and Exosphere

The possibility now exists at Arecibo to perform joint radar and optical observations of the middle and upper ionosphere/thermosphere system. As previously discussed, the 430-MHz radar can be used to measure O^+, He^+, and H^+ between 250 and 2500 km. Complimentary to this, optical observations may be made of O, He, and H over a comparable range of heights. The 6563-Å H_α intensity measurements from neutral atomic hydrogen have been measured at Arecibo for over a solar cycle [*Meriwether et al.*, 1980; *Kerr et al.*, 1986] and can be used to deduce neutral atomic hydrogen effective temperature and density profiles [*Kerr and Tepley*, 1988; *He et al.*, 1993]. Exospheric neutral helium can be observed using the 10830-Å triplet emission from metastable He [*Kerr et al.*, 1996], and exospheric neutral atomic oxygen can be observed via the 8446-Å triplet emission [*Lancaster et al.*, 1994, 2000], thus forming a complete picture of high-altitude neutral species.

Exospheric emission intensity is measured using the Earth's shadow to define the altitude of the base of the observed column emission [*Meriwether et al.*, 1980; *Kerr and Tepley*, 1988; *Nossal et al.*, 1993]. Observations are made throughout the night, during shadow rise between sunset and midnight and during shadow fall between midnight and dawn. The technique works best during winter, when twilight periods are long; at Arecibo the heights from which data are obtained can reach 25,000 km during this time period. High-resolution H_α line profiles have been used to measure effective temperatures, line asymmetry due to non-Maxwellian dynamics, and fine structure [*Meriwether et al.*, 1980; *Kerr et al.*, 1986; *Nossal et al.*, 1997, 1998].

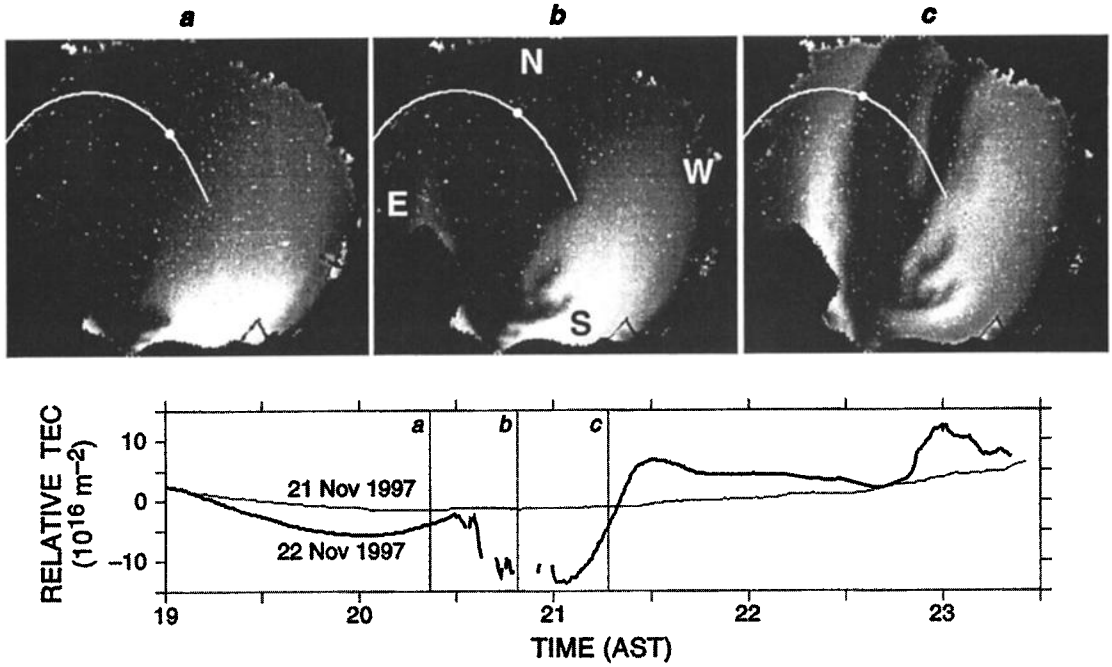

Figure 9. A set of 6300-Å all sky images showing a series of airglow bands moving northward over Arecibo during the evening of November 22–23,1997, during which Kp reached 7. The white overplots show the trajectory of GPS satellite 31 as viewed from Puerto Rico, with the solid circles indicating the points corresponding to image times and to the times marked in the total electron content (TEC) plot in the bottom panel. The darkest airglow regions are colocated with deep TEC depressions, while the bright bands have very large TEC values; this is opposite to the behavior expected from chemical arguments.

To date, observations of H_α and metastable He have been carried out at Arecibo. H_α observations from 400 to over 10,000 km have been performed using the in-house interferometers and photometers described above. Observations of metastable He between 100 and 1000 km have been carried out with a Scientific Solutions double etalon Fabry-Perot interferometer using a liquid nitrogen cooled germanium detector specifically designed for that purpose [*Kerr et al.*, 1996; *Noto et al.*, 1992]. H_α emissions have now been observed at Arecibo over a period spanning more than a solar cycle.

In addition to providing evidence of modulation and enhancement of exospheric H_α emissions by the solar cycle and following geomagnetic storms, respectively, the measurements described above are being used to study the escape of hydrogen and helium from the atmosphere [*Kerr et al.*, 1999*a*]. Helium has the lower rate of escape but is inert, and there is no known contemporary source able to replenish helium lost to space. Hydrogen, on the other hand, is replenished by sources in the lower atmosphere at a rate which depends on chemistry in both the lower and upper atmospheres as well as on transport and charge exchange in the upper atmosphere.

An understanding of both of these exoshperic processes, natural variability and escape of light atoms, is important for isolating possible long-term trends due to anthropogenic influences on climate [*CEDAR Science Steering Committee*, 1997]. For example, tropospheric methane is both one of the primary greenhouse gases and a particularly important source of topside and exospheric hydrogen, and its abundance is growing at a rate of ~1% per year. Furthermore, predictions by *Ehhalt* [1986] and the National Center for Atmospheric Research (NCAR) upper atmospheric global mean model [*Roble and Dickinson*, 1989] suggest that a doubling in the concentration of lower atmospheric methane may result in increases of 30–50% in exospheric hydrogen. Arecibo H_α data show an upward trend in emissions which appears to support the NCAR model results [*Kerr et al.*, 1999*b*]. Fabry-Perot observations from the University of Wisconsin, the other site of long-term ground-based exospheric H_α observations, also suggest an upward trend, though of lesser magnitude than that seen at Arecibo [*Nossal et al.*, 1993].

3.6. Observations of Na in the Lower E Region

Since coming on line in May 1997, the pulsed dye laser system has provided reliable resonance fluorescence lidar observations of the background neutral sodium layer. Coordinated radar/lidar meteor observations were begun during the Leonid meteor shower in November 1997 with observations of meteoric sodium at 5 s time resolution and 37.5 m range resolution and were continued

in November 1998. Future experiments will also include observations of neutral potassium, which should be particularly interesting since the nominal peak density of atmospheric potassium is about 60 atoms/cm^3, just over 1% that of sodium, whereas the meteoric contributions of the two should both be of the order of 50 atoms/cm^3, resulting in a more prominent meteoric potassium signal [*Castleberg*, 1997; *von Zahn and Höffner*, 1996].

In the past, neutral sodium lidar data taken at Arecibo have been used in conjunction with high-resolution radar data to study the relation between the occurrence of sporadic sodium layers and sporadic E [*Beatty et al.*, 1989; *Mathews et al.*, 1993; *Kane et al.*, 1993]. These studies continued when the pulsed dye lidar provided key support for several NASA sounding rockets launched from Puerto Rico in early 1998 dedicated to the study of wave and layer dynamics in the lower E region. The rockets performed in situ measurements of neutral sodium, neutral potassium, ion mass, charged dust, electric fields, and temperature. Plate 4 shows an example of the Arecibo data taken during that campaign.

4. HF Ionospheric Interaction Experiments

The Arecibo high frequency transmitter or HF facility is currently located near the Atlantic coast ~17 km NNE of the radar site [*Gordon et al.*, 1979; *Fejer et al.*, 1985; *Arecibo Observatory*, 1989; *Isham*, 1991]. Unfortunately, in September 1998, Hurricane Georges caused major damage to the antenna array; in addition, in January 1999 the government of Puerto Rico designated the surrounding area as a wetlands preserve. Taken together, these events effectively preclude continued HF operations at the current location. The future of ionospheric interaction experiments at the Arecibo Observatory is currently under study. We report here on how the facility was configured until the recent damage.

The Arecibo HF facility has frequency allocations from 2.5 to 18 MHz, although for technical reasons it has normally been used at a set of specific frequencies between 3.1 and 8.2 MHz. It can be used at 400 kW CW power and in the past has occasionally been used at 600 kW. Operations above 400 kW have been limited by the capacity of the diesel generators and the condition of the aging antenna array, which consists of two identical, adjacent, and electrically independent 4 by 4 arrays of log periodic antennas, each with a gain of 20 dB, aligned on an east-west axis. The 1994 upgrade of the HF transmission lines greatly improved the efficiency of delivering power to the antennas, with the result that the power transmitted from the array roughly doubled. The HF facility is unique among Arecibo instruments in that it is designed to actively influence the ionospheric plasma, and this powerful capability has been used to perform experiments important both for understanding the natural atmosphere and for exploring basic plasma physical processes. About one third of the roughly 1500 hours of annual atmospheric science observing time at Arecibo is normally devoted to HF interaction experiments. Selected examples of recent results are given in the remainder of this section.

4.1. Active Aeronomical Experiments

4.1.1. Artificial periodic irregularities. A method of considerable recent interest has been the artificial periodic irregularity (API) technique, in which the standing wave formed from an upgoing HF pump wave and its reflection creates quasiperiodic density and temperature irregularities having potential use as a diagnostic for vertical winds, gravity waves, and the ambient electron density profile in the F, E, and possibly D regions [*Rietveld et al.*, 1996; *Djuth et al.*, 1997*a*]. Ionospheric API observations have been performed in the past at Arecibo by *Fejer et al.* [1984] and, more recently, in June 1997. Further work is needed in order to carefully evaluate the capabilities of this new technique.

4.1.2. Ionospheric thermal balance. The ability of the Arecibo ISR to independently measure T_{O+}, T_{H+}, and T_e [*Sulzer and González*, 1996] can be used to determine the increase in these temperatures caused by HF transmissions and the rates of heat conduction between species as the temperatures relax after the HF is turned off. This is important for understanding the ionospheric thermal balance problem, and ties into the work on the ionospheric Langmuir wave equation mentioned in section 2.8.1. An initial experiment on this topic performed in January 1998 included Arecibo Fabry-Perot interferometer observations of exospheric H_α in an attempt to detect an increase in the neutral hydrogen temperature due to charge exchange with energetic H^+.

4.1.3. Accelerated electrons. HF transmissions can provide a controlled source of F region energetic electrons which the radar can then study, via their effect on the natural plasma line, as they propagate along geomagnetic field lines [*Carlson et al.*, 1982]. The improved bandwidth capabilities of the radar will significantly enhance Arecibo's capabilities for performing these measurements. In addition, electrons energized by HF transmissions excite airglow, which can be used to perform experiments in conjunction with the imagers discussed in section 3.3 [*Bernhardt et al.*, 1989*b*]. A remarkable result from an ionospheric interaction experiment performed during January 1998 indicates that the improved power output of the Arecibo HF array produced electrons of significantly higher average energy than was possible in the past [*Djuth et al.*, 1999].

4.2. Fundamental Plasma Physics: Langmuir Turbulence

The first successful F region HF interaction experiments were performed at Platteville, Colorado, in 1970. Results from these experiments led to the prediction

that plasma instabilities were excited by the electric field of the powerful HF wave [*Perkins and Kaw*, 1971] and prompted the initiation of similar experiments at Arecibo later that same year. The first HF instability enhanced plasma line spectrum was observed in 1971 by *Carlson et al.* [1972], and the first enhanced ion line spectrum was observed in 1972 by *Hagfors and Zamlutti* [1973], thus confirming the predictions. It was initially thought that parametric instabilities, a description of which can be derived from the Zakharov equations via the weak plasma turbulence approximation, would be adequate to explain the fundamental physical interaction, but it gradually became clear that the approximation was not adequate and that a full Zakharov model, which includes small-scale cavitation processes, was required [*Zakharov*, 1972; *Petviashvili*, 1976; *Fejer*, 1979; *Payne et al.*, 1984; *DuBois et al.*, 1991]. The Arecibo results of *Sulzer and Fejer* [1994] dramatically confirmed many of the features of the new model.

Plate 5, obtained using the technique of *Sulzer and Fejer* [1994], is an example of what is possible using the increased power level of the upgraded HF facility. The HF pump begins to come on at 1 ms, and a broad cavitation spectrum is seen near the top of the 1- and 2-ms subplots just below the HF reflection height, with spectral power weighted to the downshifted side of the HF pump frequency but also including upshifted enhancements. At the same time the free mode or enhanced natural Langmuir wave spectrum is seen upshifted by about 65 kHz. At 3 and 4 ms the cascading spectrum of the parametric decay mode can be at and generally downshifted from the HF pump frequency at a location known as the matching height ~1 km below the reflection height. A significant new result is the extension of the enhancements of the natural Langmuir wave spectrum downward to an altitude over 1 km below that of the cascade spectrum, seen in the negative frequency portion of the 10- and 11-ms subplots just before turnoff of the HF pump.

The variations in spectral intensity and morphology among the subplots are of particular interest, as they signal the extension of Langmuir turbulence research from the creation and development of instabilities to the microphysics of the generation and evolution of small-scale plasma irregularities. The variations are due to local focusing and defocusing of pump power in to and out of the 700 m diameter radar field of view, caused by changes in HF induced 10 m to 100 m scale size irregularities over the 10 s of real time which lapses between each subplot. As the HF wavelength is 58.8 m, the irregularities must be of this size scale in order to locally focus the HF beam. Yet the detailed height ordering of the Langmuir spectra remains undisturbed, so that the irregularities must be smaller than the 150-m range resolution of the observations. Typical F region plasma drift velocities are of the order of tens of meters per second [*Bernhardt et al.*, 1989*a*], so that an irregularity would require tens of seconds to drift through a distance comparable to the size of the radar beam. This compares well with the distance between the peaks in backscatter power seen in Plate 5, which occur at 4 and 10 ms, corresponding to a difference in real time of 60 s.

Neither enhanced Langmuir waves below the matching height nor excitation and evolution of irregularities can be fully explained by current Langmuir turbulence models; both require the incorporation of additional processes for the transfer of energy within the plasma and further work at higher modeled power densities and longer timescales. It is significant to note that in the example of Plate 5 the HF pump is exciting irregularity growth at a duty cycle of only 0.5%. Data such as these are important for shedding light on the microphysics of plasma irregularity generation. Potential applications include improving our understanding of irregularity growth in the high-latitude ionosphere due to bursts of precipitating energetic electrons as well as in other astrophysical and laboratory plasmas where rapid high-energy events are known to occur [*Robinson*, 1997].

5. Discussion

We now consider what lies ahead. Arecibo's new capabilities will contribute substantially to future scientific progress, and this is considered first, followed by comments on possibilities for future technical progress.

5.1. Future Scientific Directions

It is certain that exciting and dramatic results lay in store for future Arecibo investigations, and to best achieve those results, Arecibo will take advantage of three fundamental capabilities: first, the unsurpassed sensitivity of the incoherent scatter radar, which allows investigations of atmospheric regions and fundamental phenomena not possible at other facilities; second, the instrument cluster, which has been carefully assembled over the years by the observatory in collaboration with the national and international atmospheric, space, and plasma physics communities and which gives Arecibo significant abilities to conduct investigations that would be impossible using the radar alone; third, participation (1) as a link in the American chain of upper atmospheric observatories, (2) as a member of the international incoherent scatter radar network, and (3) as a collaborator in observational programs such as the upcoming joint National Science Foundation CEDAR (Coupling, Energetics, and Dynamics of Atmospheric Regions) and NASA TIMED (Thermosphere-Ionosphere-Mesosphere Energetics and Dynamics) satellite program, all of which enhance Arecibo's capabilities over those possible with single point investigations alone.

The potential of the Arecibo instrument cluster was dramatically demonstrated during the Coqui II rocket campaign of February, March, and April 1998, during which eight NASA sounding rockets were launched into the E region off the north coast of Puerto Rico. The

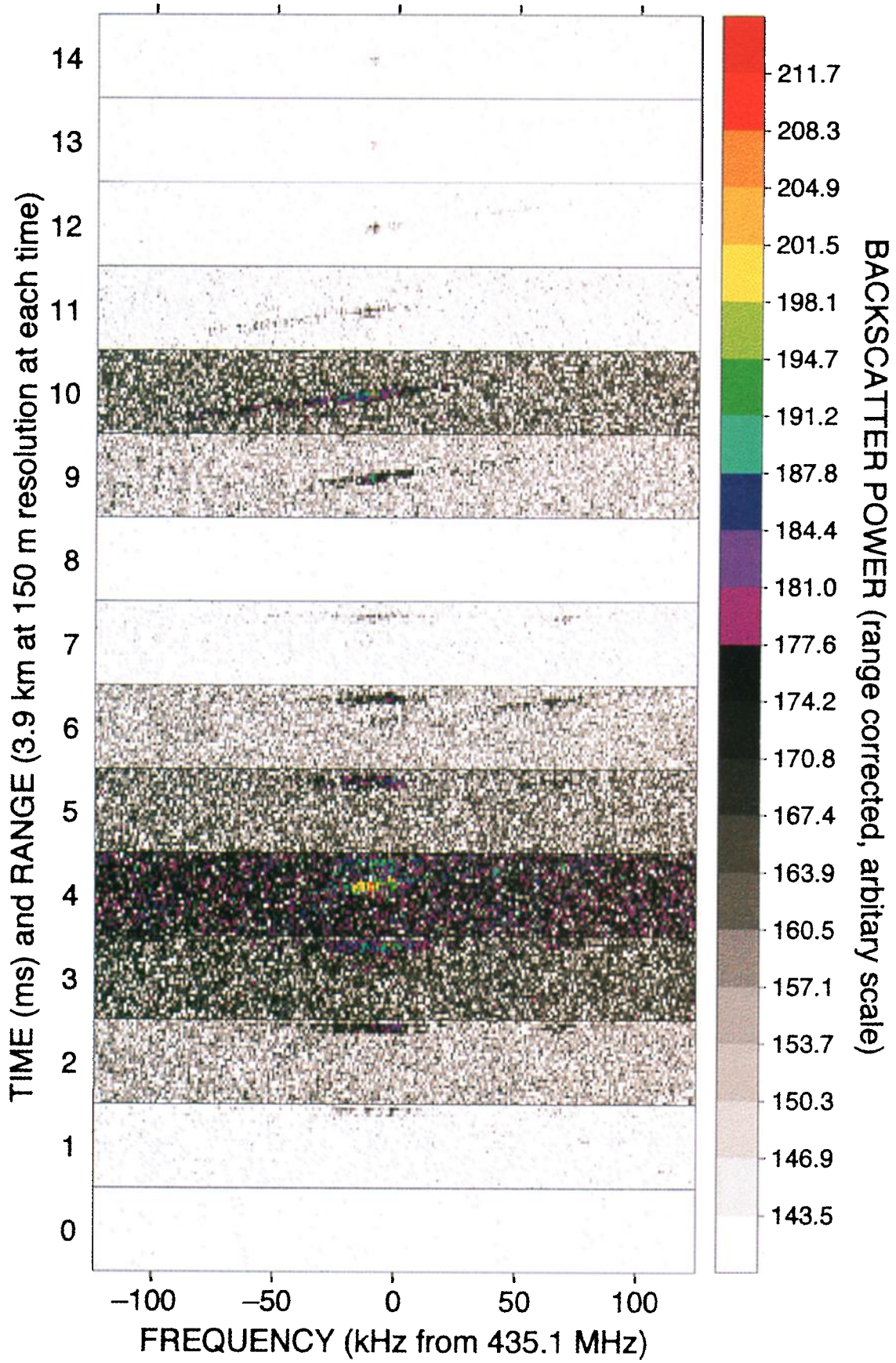
TIME (ms) and RANGE (3.9 km at 150 m resolution at each time)
14
13
12
11
10
9
8
7
6
5
4
3
2
1
0
−100
−50
0
50
100
FREQUENCY (kHz from 435.1 MHz)
211.7
208.3
204.9
201.5
198.1
194.7
191.2
187.8
184.4
181.0
177.6
174.2
170.8
167.4
163.9
160.5
157.1
153.7
150.3
146.9
143.5
BACKSCATTER POWER (range corrected, arbitary scale)

rocket experiments included several chemical releases and a flight through plasma turbulence created by the Arecibo HF facility. Arecibo's ability to perform common volume simultaneous radar and optical measurements of sudden atom layers near the turbopause transition region (see Plate 4) was the key factor in the decision of where to hold the launches. In turn, the rare combination of rocket, radar, and optical observations attracted other instruments, including one HF radar, two VHF radars, and additional imagers and cameras, which were deployed on the island during the campaign to further enhance the capabilities of the instrument cluster. Measurements made during the Coqui II campaign will contribute substantially to our understanding of the structure and dynamics of the turbopause region. We conclude the discussion of future scientific directions with a review of five key research areas in which significant progress is likely to be made.

5.1.1. Tides, waves, and turbulence. Arecibo is particularly well-suited to studies of planetary waves, tides, gravity waves, and turbulence in the mesosphere and lower thermosphere. As a CEDAR participant, as a member of the American upper atmospheric observatory chain, and with other atmospheric observatories worldwide, Arecibo is able to participate in both distributed studies of latitudinal and longitudinal coupling and cluster studies of vertical coupling vital to the understanding of the origin and evolution of these phenomena. In addition, collaborations between the TIMED satellite program and investigators using Arecibo will add longitudinal coverage to these programs.

An important example within this research area, and a topic which is likely to be the subject of focused interest for many years to come, is the study of gravity waves. How do they interact with and penetrate the wind field in the mesosphere? How do they affect ionization in the D and lower E regions? Where do they deposit their energy and momentum? The search for answers requires measurements of structure in greater detail than that which is available from observations of the mean wind field. Modern imaging technology will have a central role in the visualization of horizontal wave structure, and the plasma line technique will be used to assess vertical wave motion in the upper E region and on into the F region. Finally, dual-beam 430-MHz radar observations, scheduled to become available in 2000, will be an important part of these studies as they will reduce the time resolution of vector measurements of the thermospheric wind field from the current 16 to 8 min. Coplanar inhomogeneity measurements will be possible with a time resolution as low as 10 s (longer for difficult measurements and for observations using multiple radar programs).

Future experiments will build on the results of both special campaigns such as Coqui II and ongoing community campaigns such as the Mesosphere Lower Thermosphere Coupling Study (MLTCS). Anticipated topics include the processes by which tides and gravity waves couple the mesosphere to the lower thermosphere, the dynamics of the variability in turbopause location, and the role of dust in the formation and evolution of phenomena such as sudden atom layers, beginning with the basic question of how much dust is present in the region. Mesospheric winds, waves, and tides will be measured via sodium (dye) and potassium (Alexandrite) lidar observations, as well as with the medium-frequency (MF) radar facility. An example of upcoming collaborations includes a proposed latitudinal study of mesospheric temperatures involving Colorado State University, Arecibo, and the Institute for Atmospheric Physics in Kühlungsborn, Germany.

5.1.2. Ionospheric structure. Overlaping with the goals of and observations required for future studies of tides, waves, and turbulence are those impor-

---

Plate 5. Langmuir turbulence results produced on July 16, 1997, at 1958:05 LT using the recently doubled transmission power of the Arecibo HF ionospheric interaction facility. For this example the HF transmitter was on at a power level of 400 kW (80 MW effective isotropic radiated power) for 10 ms every 2 s. The radar pulse repetition period was 25.0025 ms, so that one data sample was taken during each HF pulse, with the time of the sample drifting 0.2 ms every 2 s. Each 1-ms subplot thus corresponds to an integration over five raw data samples spaced over 10.001 s of observing time; each subplot displays 26 range gates at 150-m range resolution for a total of 3.900 km of displayed range coverage. The upshifted plasma line was observed. The data show the principle features of Langmuir turbulence, including, just below the HF reflection height near the top of the 1- and 2-ms subplots, the broad cavitation spectrum straddling the HF pump frequency with the free mode upshifted 65 kHz and, about 1 km below the reflection height at 3 and 4 ms, the cascading spectrum of the parametric decay mode. New results include the appearance of enhancements to the natural Langmuir frequency profile at altitudes below that of the cascade spectrum, seen in the 10- and 11-ms subplots just before turnoff of the HF pump, and the significant variation in spectral intensity and morphology between the millisecond subplots, which is due to local focusing and defocusing of pump power caused by variations in HF induced 10 m to 100 m scale size irregularities over the 10 s of real time which lapses between the subplots. The variation in the background power level is due to clutter produced by the coded long pulse technique as, within each 150-m range gate, it randomizes the unwanted spectral power from adjacent gates. Thus the clutter level tracks the variation in the desired backscattered power from the Langmuir turbulence. Since the HF facility is located 17 km from the main observatory site, the radar was pointed 3.5° from zenith at an azimuth angle of 33° east of north in order to intersect the HF beam in the bottomside F region.

tant for advances in the study of ionospheric structures. The structures referred to here include those which are smaller than the characteristic scale sizes of the ionospheric medium, that is, less than the scale height vertically and less than an Earth radius horizontally. At Arecibo such studies are similar to those done by other atmospheric facilities, but because of Arecibo's midlatitude location they tend to focus on different specific phenomena.

Encompassing many phenomena in the field of ionospheric structure is the study of electrodynamics and in particular of the coupling between electric fields in the plasma and the motion of the background neutral gas. Specific topics benefiting from the instrument cluster include the fine structure of descending plasma layers and ion rain in the lower thermosphere, which could be a sign of electric coupling to other heights or may instead be due to the local actions of gravity waves. Related investigations also benefiting from coordinated distributed observations include the study of the midlatitude ionospheric response to magnetic storms and substorms and the search for processes responsible for the amplification of ionospheric disturbances, which could lead to the creation of traveling ionospheric disturbances (TIDs) and midlatitude plumes. Studies such as these are an important contribution to the worldwide effort to better understand and predict space weather.

Future dual-beam incoherent scatter radar observations will allow extremely rapid measurements of drift vectors and electric fields in two dimensions; in combination with modern airglow imaging, lidar measurements, and other optical and radio techniques, this will provide an invaluable asset for studies of ionospheric dynamics, electrodynamics, and structure. Finally, the capability of the high-frequency transmitter facility to create irregularities and cavities within the ambient plasma gives a unique degree of control over the ionospheric medium which can be used to develop a deeper understanding of the dynamics of both large- and small-scale structures.

5.1.3. Light atoms and ions. The composition and dynamics of the topside F region has become an area of considerable scientific interest, in large part due to recent studies of light ions performed at Arecibo. The sensitivity of the 430-MHz incoherent scatter radar allows routine observations to 2000 km altitude and, at times, thousands of kilometers beyond. As with the topics discussed above, the information available from the radar is magnified by the capabilities of the local instrument cluster as well as by the latitudinal coverage provided by the NSF upper atmospheric observatory chain. In addition, for topside work, longitudinal coverage is provided by other incoherent scatter radars and atmospheric observatories worldwide, and the combined data may then be used as inputs into models designed to explain and predict topside dynamics.

This combination of instrumental and modeling capabilities promises to provide fundamental advances in our understanding of neutral and ion dynamics in the topside. Important topics include topside composition, response to magnetic storms, and variations with solar cycle, as well as the classic subject of the escape of light gases and the modern field of anthropogenic global change. These topics encompass the evolution of the atmosphere on nearly all timescales and include issues of coupling from the lowest to the highest atmospheric regions as well across the full range of latitude and longitude.

Topside subject areas are clearly interrelated. For example, to understand the contributions of anthropogenic global change to topside composition and dynamics, we must first remove the variation in topside ion and neutral species with respect to season and solar flux. While we now have a basic understanding of global topside phenomena, there remains much work to do in the area of finding detailed agreement between models and observations and in understanding the origins and development of the smaller-scale processes.

5.1.4. Variability and model validation. The application of models to the understanding of atmospheric processes is not limited to the topside but is also an important area of research in middle ionospheric, thermospheric, and mesospheric physics, which in turn is tied to the topics of atmospheric dynamics and structure discussed in section 5.1.1 and 5.1.2. The validity of current models encompasses seasonal and solar cycle timescales rather than the short-term, day-to-day variation of thermospheric and F region parameters and phenomena such as temperatures, densities, drift velocities, waves, and tides. Yet it is an understanding of the nature and cause of short-term variations that is required for accurate forecasts of the effects on GPS and other satellite systems, which in turn is one of the primary goals of both phase three of the CEDAR program and of the National Space Weather Program. As we approach and pass through the new solar maximum, Arecibo will continue to contribute information needed to further advance our ability to understand and predict upper atmospheric variability.

5.1.5. HF ionospheric interactions. High-frequency radio wave ionospheric interaction experiments complement all of the areas discussed above through the development of new techniques to study aeronomy and plasma physics throughout the ionosphere. These topics range from the origin, structure, and variability of plasma irregularities of all scale sizes from the D region to the F region, to the thermal balance between charged species, to the coupling between ionospheric turbulence and magnetospheric Alfvén waves, to the detailed study of the response of the ionospheric plasma to incident electromagnetic radiation on millisecond timescales. Although Arecibo does not operate the only such high-frequency transmitter facility, nor the only one located near an incoherent scatter radar, it is uniquely situated under the relatively smooth midlatitude bottomside F region. This, in conjunction with

the sensitivity of the 430-MHz incoherent scatter radar and the extensive instrument cluster, allows studies to be performed at Arecibo that are not possible elsewhere.

5.2. Future Technical Directions

The Gregorian upgrade has provided Arecibo with improvements in radar time resolution, frequency bandwidth, system temperature, and near-field power. Significant improvements have also been made to Arecibo's optical facilities in the form of a new laboratory housing two new resonance lidar systems, to the high-frequency ionospheric interaction facility through a doubling of the transmitted power, to the medium-frequency partial reflection facility via a recent refurbishment, and to the experimental support in the form of a new digital ionosonde. In spite of these advances, in none of the three basic areas listed earlier (the sensitivity of the incoherent scatter radar, the synergistic capabilities of the local instrument cluster, and participation in the national and international observatory networks) has Arecibo reached its full potential. First, longstanding dreams of an order of magnitude increase in 430-MHz incoherent scatter radar height resolution via a transmitter bandwidth expanded from 1 to 10 MHz, as well as the ability to study the exosphere out to the plasmapause using radar power increased from 2 to 10 MW, remain to be fulfilled. Second, the international incoherent scatter radar network has expanded through the recent addition of the EISCAT Svalbard Radar, and in the next few years it is possible that a new, relocatable American incoherent scatter radar will be constructed, to be initially located in Alaska. Third, the instrument cluster continues to grow. Plans for the near future include installation of a publicly available dedicated real-time spectral processor, constructed by Geospace Research Inc. of California, to complement the wideband capability of the Gregorian feed by providing real-time data processing of coded long pulse natural plasma line data. Although a setback, the damage caused to the HF facility by Hurricane Georges also provides an opportunity for relocating to a better site and for developing an improved antenna design, which may allow for increased transmitted power density and perhaps improved frequency agility. Future possibilities for the optical program include extending lidar measurements into the daytime [*Chen et al.*, 1996] and hosting a visiting 10,830-Å resonance lidar for observations of neutral helium in the F region. More distant possibilities include upgrading the lidar receiving system to include an array of seven 0.80-m-diameter telescopes, which would extend Doppler Rayleigh lidar observations to 80 km thus overlaping with winds measured using the potassium resonance lidar, and the extension of airglow measurments to include the dayglow [*Cocks et al.*, 1980].

Finally, entirely new fields of research remain to be exploited. Solar physics, for example, would greatly benefit from the study of hitherto unobservable regions and waves in the middle corona through the construction in the western hemisphere of a large HF/VHF aperture synthesis receiving array, in conjunction with the installation of a new VHF transmitter at Arecibo, where it could take advantage of the unique gain of the 305-m dish [*James*, 1968; *Parrish*, 1968; *Isham and Rodriguez*, 1997; *Kassim and Erickson*, 1998]. Such a transmitter, with 1.5 MW or more of CW power, could also provide a second frequency, and therefore a new scale length, for incoherent scatter observations [*Watkins*, 1967; *Hagen and Behnke*, 1976] and would have potential uses for underdense ionospheric interaction experiments [*Farley*, 1963].

6. Conclusion

A review has been given of Arecibo capabilities for upper atmospheric observations. The Arecibo incoherent scatter radar and instrument cluster make a significant contribution to the American upper atmospheric observatory chain and to many other collaborative research programs while providing unmatched capabilities for local studies of microscopic and macroscopic atmospheric phenomena. Examples have been given of the observational capabilities of Arecibo radar, radio, and optical instrumentation. The current upgrading period is drawing to a close, and we look forward to new and innovative proposals for taking advantage of the national facilities available here.

Acknowledgments. The Arecibo Observatory is part of the National Astronomy and Ionosphere Center (NAIC), which is operated by Cornell University under a cooperative agreement with the National Science Foundation. We thank M. M. Davis for discussions regarding the new Gregorian feed system and related topics; C. L. Adami, I. M. Reid, and H. M. Ierkic for interesting discussions regarding the Arecibo 1.95-MHz radar; J. Y. N. Cho for information pertaining to the Arecibo 46.8-MHz radar and 430-MHz interferometer system; J. W. MacDougall for information on the Arecibo digital ionosonde; E. I. Castro, J. B. Hagen, V. Iguina, R. W. Sisk, and R. K. Zimmerman for providing information on a variety of Arecibo radio instruments; S. Nossal, S. Collins, and F. J. Garcia for informative discussions on optical observations of the exosphere, Arecibo lidar systems and observations, and the Cornell airglow imager, respectively; B. MacPherson for discussions of the 1998 solar eclipse; H. C. Carlson and F. T. Djuth for interesting discussions about the plasma line; and the Editor and referees for insightful and helpful comments. For their generous permission to use particular figures, most of them previously unpublished, we thank the following people: B. MacPherson, G. J. Bailey, F. T. Djuth, and P. Rodriguez for Plate 3; J. D. Mathews for Figure 3; F. T. Djuth for Figures 4 and 5; F. J. Garcia for Figures 8 and 9; and S. Collins for Plate 4. Figure 2 has been adapted and reprinted with the permission of Elsevier Science; Figures 5 and 6 have been adapted and reprinted with the permission of the American Geophysical Union. We thank T. Acevedo, S. Bird, H. Coffey, M. Colerico, S. Collins, F. T. Djuth, F. J. Garcia, C. Hanchett, M. Hansen, E. Lindemann, J. D. Mathews, M. Patterson, J. Powell, C. Segarra, and R. Thompson for their assistance. B.I. thanks W. E. Gordon and T. Hagfors for personal in-

spiration and for their contributions toward making radar exploration of the atmosphere and space the dynamic field that it is today; B.I. also thanks his coauthors, coworkers, and especially C. La Hoz for many interesting and illuminating discussions. This paper grew out of a presentation at the Arecibo Atmospheric Sciences Workshop, held at the Arecibo Observatory, January 9–11,1997.

Janet G. Luhmann thanks the referees for their assistance in evaluating this paper.

References

Altadill, D., and E. M. Apostolov, Vertical development of the 2-day wave in the mid-latitude ionospheric *F* region, *J. Geophys. Res.*, *103*, 29,199–29,206, 1998.

Arecibo Observatory, Arecibo Observatory user's manual, technical report, Natl. Astron. and Ionos. Cent., Arecibo Obs., Arecibo, Puerto Rico, 1989.

Baumgardner, J., B. Flynn, and M. Mendillo, Monochromatic imaging instrumentation for applications in aeronomy of the Earth and planets, *Opt. Eng.*, *32*, 3028–3032, 1993.

Beatty, T. J., R. L. Collins, C. S. Gardner, C. A. Hostetler, C. F. Sechrist Jr., and C. A. Tepley, Simultaneous radar and lidar observations of sporadic *E* and Na layers at Arecibo, *Geophys. Res. Lett.*, *16*, 1019–1022, 1989.

Behnke, R. A., *F* layer height bands in the nocturnal ionosphere over Arecibo, *J. Geophys. Res.*, *84*, 974–978, 1979.

Behnke, R. A. and R. M. Harper, Vector measurements of *F* region ion transport at Arecibo, *J. Geophys. Res.*, *78*, 8222–8234, 1973.

Bernhardt, P. A., L. M. Duncan, and C. A. Tepley, Heater-induced cavities as optical tracers of plasma drifts, *J. Geophys. Res.*, *94*, 7003–7010, 1989*a*.

Bernhardt, P. A., C. A. Tepley, and L. M. Duncan, Airglow enhancements associated with plasma cavities formed during ionospheric heating experiments, *J. Geophys. Res.*, *94*, 9071–9092, 1989*b*.

Burnside, R. G., J. C. G. Walker, and M. P. Sulzer, Kinematic properties of the *F* region ion velocity field inferred from incoherent scatter radar measuremnts at Arecibo, *J. Geophys. Res.*, *92*, 3345–3355, 1987.

Burnside, R. G., C. A. Tepley, and M. P. Sulzer, World day observations at Arecibo: 1985 to 1989, *J. Geophys. Res.*, *96*, 3691–3710, 1991*a*.

Burnside, R. G., C. A. Tepley, M. P. Sulzer, T. J. Fuller-Rowell, D. G. Torr, and R. G. Roble, The neutral thermosphere at Arecibo during geomagnetic storms, *J. Geophys. Res.*, *96*, 1289–1301, 1991*b*.

Carlson, H. C., W. E. Gordon, and R. L. Showen, High frequency induced enhancements of the incoherent scatter spectrum at Arecibo, *J. Geophys. Res.*, *77*, 1242–1250, 1972.

Carlson, H. C., V. B. Wickwar, and G. P. Mantas, Observations of fluxes of suprathermal electrons accelerated by HF excited instabilities, *J. Atmos. Terr. Phys.*, *44*, 1089–1100, 1982.

Castleberg, P. A., *Lidar development with applications to the stratosphere-troposphere exchange and tropical aerosol detection*, Ph.D. thesis, Cornell Univ., Ithaca, N. Y., 1997.

CEDAR Science Steering Committee, Coupling, energetics, and dynamics of atmospheric regions: CEDAR phase III, technical report, Atmos. Sci. Div., Nat. Sci. Found., Arlington, Va., 1997.

Chapin, E., and E. Kudeki, Radar interferometric imaging studies of long duration meteor trails observed at Jicamarca, *J. Geophys. Res.*, *99*, 8937–8949, 1994.

Chen, H., M. A. White, D. A. Krueger, and C. Y. She, Saturation spectrum of the parametric decay instability in the presence of an external magnetic field, *Opt. Lett.*, *21*, 1093–1095, 1996.

Chilson, P. B., C. W. Ulbrich, M. F. Larsen, P. Perillat, and J. E. Keener, Observations of a tropical thunderstorm using a vertically pointing, dual-frequency, collinear beam Doppler radar, *J. Atmos. Oceanic Technol.*, *10*, 663–673, 1993.

Cocks, T. D., D. F. Creighton, and F. Jacka, Application of a dual Fabry-Perot spectrometer for daytime airglow studies, *J. Atmos. Terr. Phys.*, *42*, 499–511, 1980.

Davis, M. M., Planning and Design Task Group meeting minutes number 32, technical report, Natl. Astron. and Ionos. Cent., Arecibo Obs., Arecibo, Puerto Rico, 1997.

Djuth, F. T., M. P. Sulzer, and J. H. Elder, Application of the coded long pulse technique to plasma line studies of the ionosphere, *Geophys. Res. Lett.*, *21*, 2725–2728, 1994.

Djuth, F. T., K. M. Groves, J. H. Elder, E. R. Shinn, J. M. Quinn, J. Villasenor, and A. Y. Wong, Measurements of artificial periodic inhomogeneities at HIPAS, *J. Geophys. Res.*, *102*, 24,023–24,035, 1997*a*.

Djuth, F. T., M. P. Sulzer, J. H. Elder, and V. B. Wickwar, High resolution studies of atmosphere-ionosphere coupling at Arecibo Observatory, Puerto Rico, *Radio Sci.*, *32*, 2321–2344, 1997*b*.

Djuth, F. T., et al., Large airglow enhancements produced via wave-plasma interactions in sporadic *E*, *Geophys. Res. Lett.*, *26*, 1557–1560, 1999.

Dougherty, J. P., and D. T. Farley, A theory of incoherent scattering of radio waves by a plasma, 3, Scattering in a partly ionized gas, *J. Geophys. Res.*, *68*, 5473–5486, 1963.

DuBois, D. F., H. A. Rose, and D. Russell, Coexistence of parametric decay cascades and caviton collapse at subcritical densities, *Phys. Rev. Lett.*, *66*, 1970–1973, 1991.

Eather, R. H., and D. L. Reasoner, Spectrophotometry of faint light sources with a tilting-filter photometer, *Appl. Opt.*, *8*, 227–242, 1969.

Ehhart, D. H., On the consequence of a tropospheric CH_4 increase to the exospheric density, *J. Geophys. Res.*, *91*, 2843, 1986.

Erickson, P. J., and W. E. Swartz, Mid-latitude incoherent scatter observations of helium and hydrogen ions, *Geophys. Res. Lett.*, *21*, 2745–2748, 1994.

Evans, J. V., Radio echo studies of meteors at 68-centimeter wavelength, *J. Geophys. Res.*, *70*, 5395–5416, 1965.

Evans, J. V., Radar observations of meteor deceleration, *J. Geophys. Res.*, *71*, 171–188, 1966.

Evans, J. V., Theory and practice of ionosphere study by Thomson scatter radar, *Proc. IEEE*, *57*, 498–530, 1969.

Farley, D. T., Artificial heating of the electrons in the *F* region of the ionosphere, *J. Geophys. Res.*, *68*, 401–413, 1963.

Farley, D. T., Multiple pulse incoherent scatter correlation function measurements, *Radio Sci.*, *7*, 661–666, 1972.

Fejer, J. A., Ionospheric modification and parametric instabilities, *Rev. Geophys.*, *17*, 135–153, 1979.

Fejer, J. A., H. M. Ierkic, R. F. Woodman, J. Röttger, M. Sulzer, R. A. Behnke, and A. Veldhuis, Observations of the HF-enhanced plasma line with a 46.8-MHz radar and reinterpretation of previous observations with the 430-MHz radar, *J. Geophys. Res.*, *88*, 2083–2092, 1983.

Fejer, J. A., F. T. Djuth, and C. A. Gonzales, Bragg backscatter from plasma inhomogeneities due to a powerful ionospherically reflected radio wave, *J. Geophys. Res.*, *89*, 9145–9147, 1984.

Fejer, J. A., C. A. Gonzales, H. M. Ierkic, M. P. Sulzer, C. A. Tepley, L. M. Duncan, F. T. Djuth, S. Ganguly, and W. E. Gordon, Ionospheric modification experiments with the Arecibo heating facility, *J. Atmos. Terr. Phys.*, *47*, 1165–1179, 1985.

Friedman, J. S., C. A. Tepley, P. A. Castleberg, and H. Roe, Middle atmospheric Doppler lidar using an iodine vapor edge filter, *Opt. Lett.*, *22*, 1648–1650, 1997.

Friedman, J. S., S. A. González, C. A. Tepley, Q. H. Zhou, M. P. Sulzer, S. C. Collins, and B. W. Grime, Simultaneous atomic and ion layer enhancements in the mesopause region during the Coqui II sounding rocket campaign, *Geophys. Res. Lett.*, *27*, 449–452, 2000.

Fujitaka, K., and T. Tohmatsu, A tidal theory of the ionospheric intermediate layer, *J. Atmos. Terr. Phys.*, *35*, 425–438, 1973.

Fukao, S., M. C. Kelley, T. Shirakawa, T. Takami, M. Yamamoto, T. Tsuda, and S. Kato, Turbulent upwelling of the midlatitude ionosphere, 1, Observational results by the MU radar, *J. Geophys. Res.*, *96*, 3725–3746, 1991.

Garcia, F. J., M. J. Taylor, and M. C. Kelley, Two dimensional spectral analysis of mesospheric airglow image data, *Appl. Opt.*, *36*, 7375–7385, 1997.

Goldsmith, P. F., The second Arecibo upgrade, *IEEE Potentials*, *15*(3), 38–43, 1996.

González, S. A., and M. P. Sulzer, Detection of He^+ layering in the topside ionosphere over Arecibo during equinox solar minimum conditions, *Geophys. Res. Lett.*, *23*, 2509–2512, 1996.

Gordon, W. E., Incoherent scattering of radio waves by free electrons with applications to space exploration by radar, *Proc. IRE*, *46*, 1824–1829, 1958.

Gordon, W. E., Arecibo ionospheric observatory, *Science*, *146*, 26–30, 1964.

Gordon, W. E., F. T. Djuth, and L. M. Duncan, Final technical report, full scale power density test definition for studying ionosphere/magnetosphere microwave-beam interactions at Arecibo, Puerto Rico, Task 1, Design of the heating experiment, technical report, Rice Univ., Houston, Tex., 1979.

Gordon, W. E., R. Showen, and H. C. Carlson, Ionospheric heating at Arecibo: First tests, *J. Geophys. Res.*, *76*, 7808–7813, 1971.

Hagen, J. B., and R. A. Behnke, Detection of the electron componenet of the spectrum in incoherent scatter of radio waves by the ionosphere, *J. Geophys. Res.*, *81*, 3441–3443, 1976.

Hagfors, T., Incoherent scatter observations of the plasma line with a chirped pulse system, *Radio Sci.*, *17*, 727–734, 1982.

Hagfors, T., and R. A. Brockelman, A theory of collision dominated electron density fluctuations in a plasma with applications to incoherent scattering, *Phys. Fluids*, *14*, 1143–1151, 1971.

Hagfors, T., and C. J. Zamlutti, Observation of enhanced ion line frequency spectrum during Arecibo ionospheric modification experiment, *AGARD Conf. Proc.*, *138*, 5-1–5-11, 1973.

Harper, R. M., Preliminary measurements of the ion component of the incoherent scatter spectrum in the 60–90 km region over Arecibo, *Geophys. Res. Lett.*, *5*, 784–786, 1978.

He, X., R. B. Kerr, J. Bishop, and C. A. Tepley, Determining exospheric hydrogen density by reconciliation of H_α measurements with radiative transfer theory, *J. Geophys. Res.*, *98*, 21,611–21,626, 1993.

Herrero, F. A., and J. W. Meriwether Jr., 6300 Å airglow meridional intensity gradients, *J. Geophys. Res.*, *85*, 4191–4204, 1980.

Hines, C. O., G. W. Adams, J. W. Brosnahan, F. T. Djuth, M. P. Sulzer, and C. A. Tepley, Multiinstrument observations of mesospheric motions over Arecibo: Comparisons and interpretations, *J. Atmos. Terr. Phys.*, *55*, 241–287, 1993.

Holden, D. N., C. W. Ulbrich, and M. F. Larsen, UHF and VHF radar observations of thunderstorms, *Handb. MAP*, *20*, 288–292, 1986.

Ierkic, H. M., R. F. Woodman, and P. Perillat, Ultrahigh vertical resolution radar measurements in the lower stratosphere at Arecibo, *Radio Sci.*, *25*, 941–952, 1990.

Ingham, M. F., The spectrum of the airglow, *Sci. Am.*, *226*(1), 78–85, 1972.

International Space Environment Service (ISES), International geophysical calendar 1997, *Radio Sci. Bull.*, *279*, 17–20, Dec. 1996.

Isham, B., *Chirped incoherent scatter radar observations of the HF-modified ionosphere*, Ph.D. thesis, Cornell Univ., Ithaca, N. Y., 1991.

Isham, B., and P. Rodriguez, Prospects for ground-based solar radar observations in the International Solar-Terrestrial Program era, *Eos Trans. AGU*, *78*(17), Spring Meet. Suppl., S258, 1997.

James, J. C., Radar studies of the Sun, *Radar Astronomy*, edited by J. V. Evans and T. Hagfors, pp. 323–385, McGraw-Hill, New York, 1968.

Kane, T. J., C. S. Gardner, Q. H. Zhou, J. D. Mathews, and C. A. Tepley, Lidar, radar, and airglow observations of a prominent sporadic Na/sporadic *E* layer event at Arecibo during AIDA-89, *J. Atmos. Terr. Phys.*, *55*, 499–511, 1993.

Kassim, N. E., and W. C. Erickson, Meter/decameter wavelength array for astrophysics and solar radar, *Proc. SPIE*, *3357*, 740–754, 1998.

Kelley, M. C., and S. Fukao, Turbulent upwelling of the midlatitude ionosphere, 2, Theoretical framework, *J. Geophys. Res.*, *96*, 3747–3753, 1991.

Kelley, M. C., and C. A. Miller, Electrodynamics of midlatitude spread *F*, 3, Electrohydrodynamic waves? A new look at the role of electric fields in thermospheric wave dynamics, *J. Geophys. Res.*, *102*, 11,539–11,547, 1997.

Kerdock, A. M., R. Mayer, and D. Bass, Longest binary pulse compression codes with given peak sidelobe levels, *Proc. IEEE*, *74*, 366, 1986.

Kerr, R. B., and C. A. Tepley, Ground-based measurements of exospheric hydrogen density, *Geophys. Res. Lett.*, *15*, 1329–1332, 1988.

Kerr, R. B., S. K. Atreya, J. W. Meriwether, Jr., C. A. Tepley, and R. G. Burnside, Simultaneous H_α line profile and radar measurements at Arecibo, *J. Geophys. Res.*, *91*, 4491–4512, 1986.

Kerr, R. B., J. Noto, R. S. Lancaster, M. Franco, R. J. Rudy, R. Williams, and J. H. Hecht, Fabry-Perot observations of helium 10830 Å emission at Millstone Hill, *Geophys. Res. Lett.*, *23*, 3239–3242, 1996.

Kerr, R. B., R. Garcia, X. He, R. S. Lancaster, J. Noto, R. A. Doe, C. A. Tepley, M. Lappen, B. McCormack, and J. S. Friedman, Periodic variations of geocoronal Balmer α brightness due to solar-driven exospheric abundance variations, *J. Geophys. Res.*, in press, 2000*a*.

Kerr, R. B., X. He, R. S. Lancaster, J. Noto, R. A. Doe, M. Lappen, B. McCormack, C. A. Tepley, R. Garcia, and J. S. Friedman, Secular variability of the geocoronal Balmer α brightness: Magnetic activity and possible human influences, *J. Geophys. Res.*, in press, 2000*b*.

Kildal, P., and M. M. Davis, Characterisation of near-field focusing with application to low altitude beam focusing of the Arecibo tri-reflector system, *IEE Proc. Part H Microwave Antennas Propag.*, *143*(4), 284–292, 1996.

Kildal, P., L. Baker, and T. Hagfors, Development of a dual reflector feed for the Arecibo radio telescope: An overview, *IEEE Antennas Propag. Mag.*, *33*, 12–17, 1991.

Kildal, P., L. Baker, and T. Hagfors, The Arecibo upgrading:

Electrical design and expected performance of the dual reflector feed system, *Proc. IEEE*, *82*, 714–724, 1994.

Kofman, W., J. St.-Maurice, and A. P. van Eyken, Heat flow effect on the plasma line frequency, *J. Geophys. Res.*, *98*, 6079–6085, 1993.

Kohl, H., and M. T. Rietveld, Harmonics of the ion acoustic frequency in the heater induced ion spectrum, *J. Geophys. Res.*, *101*, 5391–5395, 1996.

LaLonde, L. M., The upgraded Arecibo Observatory, *Science*, *186*, 213–218, 1974.

Lancaster, R. S., R. B. Kerr, K. Ng, J. Noto, M. Franco, and S. C. Solomon, Recent observations of the OI 8446 Å emission over Millstone Hill, *Geophys. Res. Lett.*, *21*, 829–832, 1994.

Lancaster, R. S., R. B. Kerr, L. S. Waldrop, J. Noto, S. C. Solomon, C. A. Tepley, R. Garcia, and J. Friedman, Brightness measurements of the nighttime OI 8446 Å airglow emission from the Millstone Hill and Arecibo observatories, *J. Geophys. Res.*, in press, 2000.

Lehtinen, M. S., and I. Häggström, A new modulation principle for incoherent scatter radars, *Radio Sci.*, *22*, 625–634, 1987.

MacDougall. J. W., G. E. Halland, and K. Hayashi, *F* region gravity waves in the central polar cap, *J. Geophys. Res.*, *102*, 14,513–14,530, 1997.

Mathews, J. D., Sporadic e: Current views and recent progress, *J. Atmos. Sol. Terr. Phys.*, pages 413–435, 1998.

Mathews, J. D., Q. H. Zhou, C. R. Philbrick, Y. T. Morton, and C. S. Gardner, Observations of ion and sodium coupled processes during AIDA, *J. Atmos. Terr. Phys.*, *55*, 487–498, 1993.

Mathews, J. D., D. D. Meisel, K. P. Hunter, V. S. Getman, and Q. H. Zhou, Very high resolution studies of micrometeors using the Arecibo 430 MHz radar, *Icarus*, *126*, 157–169, 1997*a*.

Mathews, J. D., M. P. Sulzer, and P. Perillat, Aspects of layer electrodynamics revealed by high resolution observations of the 80–270 km ionosphere, *Geophys. Res. Lett.*, *24*, 1411–1414, 1997*b*.

Measures, R. M., *Laser Remote Sensing: Fundamentals and Applications*, Krieger, Malabar, Fl., 1984.

Mendillo, M., J. Baumgardner, D. Nottingham, J. Aarons, B. Reinisch, J. Scali, and M. Kelley, Investigations of thermospheric-ionospheric dynamics with 6300-Å images from the Arecibo Observatory, *J. Geophys. Res.*, *102*, 7331–7343, 1997.

Meriwether, J. W., Jr., D. G. Torr, J. C. G. Walker, and A. O. Nier, The $O^+(^2P)$ emission at 7320 Å in twilight, *J. Geophys. Res.*, *83*, 3311–3319, 1978.

Meriwether, J. W., Jr., S. K. Atreya, T. M. Donahue, and R. G. Burnside, Measurements of the spectral profile of Balmer α emission from the hydrogen geocorona, *Geophys. Res. Lett.*, *7*, 967–970, 1980.

Miller, C. A., W. E. Swartz, M. C. Kelley, M. Mendillo, D. Nottingham, J. Scali, and B. Reinisch, The electrodynamics of midlatitude spread *F*, 1, Observations of unstable, gravity wave induced ionospheric electric fields at tropical latitudes, *J. Geophys. Res.*, *102*, 11,521–11,532, 1997.

Muldrew, D. B., The formation of ducts and spread *F* and the initiation of bubbles by field-aligned currents, *J. Geophys. Res.*, *85*, 613–625, 1980.

Nelson, G. J., and L. L. Cogger, Dynamical behaviour of the nighttime ionosphere at Arecibo, *J. Atmos. Terr. Phys.*, *33*, 1711–1726, 1971.

Nossal, S., R. J. Reynolds, F. L. Roesler, F. Scherb, and J. Harlander, Solar cycle variations of geocoronal Balmer α emission, *J. Geophys. Res.*, *98*, 3669–3676, 1993.

Nossal, S., F. L. Roesler, M. M. Coakley, and R. J. Reynolds, Geocoronal hydrogen Balmer α line profiles obtained using Fabry-Perot annular summing spectroscopy: Effective temperature results, *J. Geophys. Res.*, *102*, 14,541–14,553, 1997.

Nossal, S., F. L. Roesler, and M. M. Coakley, Cascade excitation in the geocoronal hydrogen Balmer α line, *J. Geophys. Res.*, *103*, 381–390, 1998.

Noto, J., R. B. Kerr, K. Ng, R. S. Lancaster, and M. Dorin, Transportable broad-bandpass Fabry-Perot spectrometer for solar system observations, *Proc. SPIE*, *1745*, 192–198, 1992.

Ostro, S. J., Planetary radar astronomy, *Rev. Mod. Phys.*, *65*(4), 1235–1279, 1993.

Palmer, R. D., M. F. Larsen, P. B. Howell, J. Y. N. Cho, R. M. Narayanan, and M. C. Kelley, A new spatial interferometry capability using the Arecibo 430 MHz radar, *Radio Sci.*, *32*, 749–755, 1997.

Palo, S. E., et al., An intercomparison between the GSWM, UARS, and ground based radar observations: A case study in January 1993, *Ann. Geophys.*, *15*, 1123–1141, 1997.

Parrish, A., Solar radar experiments, 1967, *Tech. Rep. 300*, 20 pp., Cent. for Radiophys. and Space Res., Cornell Univ., Ithaca, N. Y., 1968.

Payne, G. L., D. R. Nicholson, R. M. Downie, and J. P. Sheerin, Modulational instability and soliton formation during ionospheric heating, *J. Geophys. Res.*, *89*, 10,921–10,928, 1984.

Pellinen-Wannberg, A., and G. Wannberg, Meteor observations with the European incoherent scatter UHF radar, *J. Geophys. Res.*, *99*, 11379–11390, 1994.

Perkins, F. W., Spread *F* and ionospheric currents, *J. Geophys. Res.*, *78*, 218–226, 1973.

Perkins, F. W., and P. K. Kaw, On the role of plasma instabilities in ionospheric heating by radio waves, *J. Geophys. Res.*, *76*, 282–284, 1971.

Petviashvili, V. I., Formation of three-dimensional Langmuir solitons by an intense radio wave in the ionosphere, *Sov. J. Plasma Phys.*, Engl. Transl., *2*, 247–249, 1976.

Rastogi, P. K., J. D. Mathews, W. Ying, and J. Röttger, Simultaneous VHF and UHF radar observations of the mesosphere at Arecibo during a solar flare: A check on the gradient-mixing hypothesis, *Radio Sci.*, *23*, 97–105, 1988.

Reid, I. M., MF Doppler and spaced antenna radar measurements of upper middle atmosphere winds, *J. Atmos. Terr. Phys.*, *50*, 117–134, 1988.

Rietveld, M. T., E. Turunen, H. Matveinen, N. P. Goncharov, and P. Pollari, Artificial periodic irregularities in the auroral ionosphere, *Ann. Geophys.*, *14*, 1437–1453, 1996.

Robinson, P. A., Nonlinear wave collapse and strong turbulence, *Rev. Mod. Phys.*, *69*(2), 507–573, 1997.

Roble, R. G., and R. E. Dickinson, How will changes in carbon dioxide and methane modify the mean structure of the mesosphere and thermosphere?, *Geophys. Res. Lett.*, *16*, 1441–1444, 1989.

Röttger, J., P. Czechowski, and G. Schmidt, First low power VHF radar observations of tropospheric, stratospheric and mesospheric winds and turbulence at the Arecibo Observatory, *J. Atmos. Terr. Phys.*, *43*, 789–800, 1981.

Röttger, J., H. M. Ierkic, R. K. Zimmerman, and J. Hagen, Investigations of the lower and middle atmosphere at the Arecibo Observatory and a description of the new VHF radar project, *Handb. MAP*, *20*, 349–358, 1986.

Sato, T., and R. F. Woodman, Fine altitude resolution observations of stratospheric turbulent layers by the Arecibo 430 MHz radar, *J. Atmos. Sci.*, *39*, 2546–2552, 1982.

She, C. Y., and J. R. Yu, Simultaneous three frequency na lidar measurements of radial wind and temperature in

the mesopause region, *Geophys. Res. Lett.*, *21*, 1771–1774, 1994.

Showen, R. L., The spectral measurement of plasma lines, *Radio Sci.*, *14*, 503–508, 1979.

Sulzer, M. P., A phase modulation technique for a sevenfold statistical improvement in incoherent scatter data taking, *Radio Sci.*, *21*, 737–744, 1986*a*.

Sulzer, M. P., A radar technique for high range resolution incoherent scatter autocorrelation function measurements utilizing the full average power of klystron radars, *Radio Sci.*, *21*, 1033–1040, 1986*b*.

Sulzer, M. P., and J. A. Fejer, Radar spectral observations of HF-induced ionospheric Langmuir turbulence with improved range and time resolution, *J. Geophys. Res.*, *99*, 15035–15050, 1994.

Sulzer, M. P., and S. A. González, Simultaneous measurements of O^+ and H^+ temperatures in the topside ionosphere over Arecibo, *Geophys. Res. Lett.*, *23*, 3235–3238, 1996.

Sürücü, F., S. J. Franke, and E. Kudeki, On the influence of specular reflections in MF radar wind measurements, *Radio Sci.*, *30*, 1229–1244, 1995.

Taylor, M. J., and F. J. Garcia, A two-dimensional spectral analysis of short-period gravity waves imaged in the OI (557.7 nm) and near-infrared OH nightglow emissions over Arecibo, Puerto Rico, *Geophys. Res. Lett.*, *22*, 2473–2476, 1995.

Tepley, C. A., Spectrophotometric measurement techniques of weak emissions in twilight airglow, *WITS Handb.*, *2*, pp. 224–249, SCOSTEP Secr., Univ. of Ill., Urbana, 1989.

Tepley, C. A., The Doppler Rayleigh lidar system at Arecibo, *IEEE Trans. Geosci. Remote Sens.*, *31*, 36–47, 1993.

Tepley, C. A., Neutral winds of the middle atmosphere observed at Arecibo using a Doppler Rayleigh lidar, *J. Geophys. Res.*, *99*, 25,781–25,790, 1994.

Tepley, C. A., R. G. Burnside, and J. W. Meriwether Jr., Horizontal thermal structure of the mesosphere from observations of OH(8-3) band emissions, *Planet. Space Sci.*, *29*, 1241–1249, 1981.

Thomson, J. J., *Conduction of Electricity through Gases*, Cambridge Univ. Press, New York, 1906.

Vincent, R. A., and D. Lesicar, Dynamics of the equatorial mesosphere: First results with a new generation partial reflection radar, *Geophys. Res. Lett.*, *18*, 825–828, 1991.

von Zahn, U., and J. Höffner, Mesopause temperature profiling by potassium lidar, *Geophys. Res. Lett.*, *23*, 141–144, 1996.

Watkins, C. D., Notes on the use of the 40 MHz radar for ionospheric incoherent scatter experiments at Arecibo, *Technical Report CRSR 271*, Cent. for Radiophys. and Space Res., Cornell Univ., Ithaca, N. Y., 1967.

Wickwar, V. B., *Photoelectrons from the magnetic conjugate point: Studies by means of the 6300 predawn enhancement and the plasma line enhancement*, Ph.D. thesis, Rice Univ., Houston, Tex., 1971.

Woodman, R. F., High altitude-resolution stratospheric measurements with the Arecibo 2380 MHz radar, *Radio Sci.*, *15*, 423–430, 1980.

Yngvesson, K. O., and F. W. Perkins, Radar Thomson scatter studies of photoelectrons in the ionosphere and Landau damping, *J. Geophys. Res.*, *73*, 97–110, 1968.

Zakharov, V. E., Collapse of Langmuir waves, *Sov. Phys. JETP*, Engl. Transl., *35*, 908–914, 1972.

Zhou, Q. H., Two day oscillation of electron concentration in the lower ionosphere, *J. Atmos. Sol. Terr. Phys.*, *60*, 1669–1677, 1998.

Zhou, Q. H. and J. D. Mathews, A spectral technique for the detection and correction of coherent interference effects on incoherent scatter radar power profiles, *Radio Sci.*, *29*, 1173–1177, 1994.

Zhou, Q. H., and M. P. Sulzer, Incoherent scatter radar observation of the *F* region ionosphere at Arecibo during January 1993, *J. Atmos. Sol. Terr. Phys.*, *59*, 2213–2229, 1997.

Zhou, Q. H., C. A. Tepley, and M. P. Sulzer, Meteor observations by the Arecibo 430 MHz incoherent scatter radar, I, Results from time-integrated observations, *J. Atmos. Terr. Phys.*, *57*, 421–431, 1995.

Zhou, Q. H., M. P. Sulzer, S. A. González, J. S. Friedman, C. A. Tepley, J. Y. N. Cho, and B. Isham, Coordinated incoherent scatter radar and optical observations during the world days during 1997-98, A proposal to the National Astronomy and Ionosphere Center, technical report, Natl. Astron. and Ionos. Cent., Arecibo Obs., Arecibo, Puerto Rico, 1997*a*.

Zhou, Q. H., M. P. Sulzer, and C. A. Tepley, An analysis of tidal and planetary waves in the neutral winds and temperature observed at low latitude *E* region heights, *J. Geophys. Res.*, *102*, 11,491–11,505, 1997*b*.

Zhou, Q. H., M. P. Sulzer, C. A. Tepley, C. G. Fesen, R. G. Roble, and M. C. Kelley, Neutral winds and temperature at the lower thermosphere and mesosphere during January 1993: Observations and comparison with TIME-GCM, *J. Geophys. Res.*, *102*, 11,507–11,519, 1997*c*.

Zhou, Q. H., P. Perrilat, J. Y. N. Cho, and J. D. Mathews, Simultaneous meteor echo observations by large-aperture VHF and UHF radars, *Radio Sci.*, *33*, 1641–1654, 1998.

Zhou, Q. H., J. D. Mathews, and Q. N. Zhou, Incoherent scatter radar study of the impact of the meteoric influx on the nocturnal *E* region ionization, *Geophys. Res. Lett.*, *26*, 1833–1836, 1999*a*.

Zhou, Q. H., Q. N. Zhou, and J. D. Mathews, Arithmetic average, geometric average and ranking: Application to incoherent scatter radar data processing, *Radio Sci.*, *34*, 1227–1237, 1999*b*.

Zhou, Q. H., H. Monroy, D. C. Fritts, H. M. Ierkic, B. Isham, J. R. Isler, and S. E. Palo, Radar observations of longitudinal variability of tidal/planetary waves and mean motions in the tropical mesosphere, *J. Geophys. Res.*, *105*, 2151–2161, 2000.

J. S. Friedman, S. A. González, M. P. Sulzer, C. A. Tepley, and Q. H. Zhou, Atmospheric Sciences Group, Arecibo Observatory, HC3 Box 53995, Arecibo, PR 00612. (jonathan@naic.edu; sixto@naic.edu; msulzer@naic.edu; ctepley@naic.edu; zhou@naic.edu)

B. Isham, Department of Natural Sciences and Mathematics, Interamerican University, Route 830 Number 500 Office E121, Bayamón, PR 00957. (bisham@bc.inter.edu)

M. C. Kelley, Department of Electrical Engineering, Cornell University, 318 Rhodes Hall, Ithaca, NY 14853-5401. (mikek@ee.cornell.edu)

(Received October 8, 1997; revised July 12, 1999; accepted July 13, 1999.)